J. Fluid Mech. (2015), *vol.* 764, *pp.* 316–348.
doi:10.1017/jfm.2014.709

Thermomagnetic convection in a layer of ferrofluid placed in a uniform oblique external magnetic field

Habibur Rahman[1] **and Sergey A. Suslov**[1,†]

[1]Department of Mathematics, H38, Swinburne University of Technology, John Street, Hawthorn, VIC 3122, Australia

(Received 8 August 2014; revised 20 November 2014; accepted 3 December 2014; first published online 5 January 2015)

Linear stability of magnetoconvection of a ferromagnetic fluid contained between two infinite differentially heated non-magnetic plates in the presence of an oblique uniform external magnetic field is studied in zero gravity conditions. The thermomagnetic convection that arises is caused by the spatial variation of magnetisation occurring due to its dependence on the temperature. The critical values of the governing parameters at which the transition between motionless and convective states is observed are determined for various field inclination angles and for fluid magnetic parameters that are consistently chosen from a realistic experimental range. It is shown that, similar to natural paramagnetic fluids, the most prominent convection patterns align with the in-layer component of the applied magnetic field but in contrast to such paramagnetic fluids the instability patterns detected in ferrofluids can be oscillatory. It is also found that, contrary to paramagnetic fluids, the stability characteristics of magnetoconvection in ferrofluids depend on the magnitude of the applied field which becomes an additional parameter of the problem. This is shown to be due to the nonlinearity of the magnetic field distribution within the ferrofluid.

Key words: magnetic fluids, magneto convection, MHD and electrohydrodynamics

1. Introduction

Synthetic magnetic fluids, also known as ferrofluids, are stable colloidal suspensions consisting of the carrier liquid (kerosene, water or mineral oil) and magnetic (iron, cobalt, nickel etc.) nanoparticles. The most widely studied ferrofluids, however, are based on colloidal magnetite (Fe_3O_4). Generally, the suspended ultra-fine magnetite particles with diameter d_p of the order of 10 nm are coated with a surfactant layer preventing them from forming aggregates. Due to demagnetisation and chemical sorption effects there is also a layer of demagnetised magnetite of thickness $\sim$1 nm at the boundary of the magnetic core.

Studies on the magnetic properties of such colloids have been conducted since the 1930s (Elmore 1938) but they intensified noticeably, starting from the 1960s and 1970s (Finlayson 1970; Bogatyrev & Shaidurov 1976), when the industrial

† Email address for correspondence: ssuslov@swin.edu.au

production of magnetic fluids became possible. Currently, a significant body of literature exists devoted to the properties of ferrofluids, see, for example, Rosensweig (1979, 1985), Bashtovoy, Berkovsky & Vislovich (1988), Blums, Cebers & Maiorov (1997), Odenbach (2009) and references therein. In the absence of a magnetic field, magnetic moments of individual particles in a ferrofluid are randomly oriented so that the fluid has no net magnetisation. However, when placed in a magnetic field, they orient along the applied field and the fluid becomes magnetised. The degree of magnetisation depends on the strength of the applied field and the local temperature and concentration of magnetic particles. Driven by the Kelvin force that arises, a magnetised fluid tends to flow toward regions with a stronger magnetic field. Such a fluid motion is referred to as magnetoconvection. It does not require gravity to be initiated in a non-uniformly heated fluid and can be conveniently controlled by varying the applied external magnetic field (Schwab, Hildebrandt & Stierstadt 1983; Tangthieng *et al.* 1999; Bozhko & Putin 2003, 2009; Zablotsky, Mezulis & Blums 2009). Therefore it is considered to be an important alternative to gravitational convection in heat exchange systems where natural convection cannot arise due to the lack of gravity (orbital stations) (Odenbach 1995; Bozhko & Putin 2009) or extreme confinement (microelectronics) (Matsuki & Murakami 1987; Mukhopadhyay *et al.* 2005; Koji, Hideaki & Masahiro 2007; Lian, Xuan & Li 2009). Thus in the current study we focus on features of a pure magnetic convection by setting the gravitational acceleration to zero in the governing equations. This also allows us to reduce the number of governing parameters of the problem to keep this paper to a reasonable length. The results we have obtained for mixed magneto-gravitational convection regimes will be reported in a separate publication.

Consistent with our previous studies (Suslov 2008; Suslov *et al.* 2012) we consider a planar geometry: a fluid layer confined by long and wide non-magnetic plates. The choice of such a classical geometry is dictated by a number of factors. Firstly, it is a common prototype configuration for realistic heat exchangers. Secondly, it allows one to make significant analytical and computational progress without being overwhelmed by geometrical details. Thirdly, this geometry is relatively easy to realise in experiments. An alternative setup that has been extensively studied numerically consists of two coaxial co-rotating or differentially rotating cylinders (e.g. Zebib 1996; Tagg & Weidman 2007; Altmeyer *et al.* 2010). However as mentioned in Suslov *et al.* (2010) experimental implementation of such a geometry is somewhat more complicated and the magnetic field applied in this case is necessarily non-uniform, which complicates the understanding of basic thermomagnetic mechanisms that are of interest here.

There are a number of motivating factors for this study stemming from experimental observations reported by our collaborators (Bozhko & Putin 1991; Bozhko *et al.* 1998; Bozhko & Putin 2003; Suslov *et al.* 2012). In particular, it has been observed that when a normal magnetic field is applied to a sufficiently wide and long ferrofluid layer the convection patterns arising near the edges of the experimental layer differ drastically in both orientation and behaviour from their counterparts in the central part of the layer. Namely, while the most prominent pattern in the middle part of the layer is stationary, propagating structures have been detected near the edges that form some angle with the boundary, see figure 9 in Suslov *et al.* (2012). The exact reasons for such a different behaviour of a ferrofluid near the edges of the flow domain remain unclear to date and our present study explores one of the plausible explanations. At the boundary between magnetic (ferrofluid) and non-magnetic (container wall) media the magnetic field lines inevitably refract, which is the consequence of Maxwell's

boundary conditions for a magnetic field, see § 2. As a result, even if the applied magnetic field is assumed to be normal to the layer, which was the case in the majority of previous studies (e.g. Finlayson 1970; Suslov 2008), the field lines necessarily curve near the layer edges so that they are effectively 'sucked into' the magnetic medium. Such a behaviour of magnetic field lines near the borders is very sensitive to the minor details of the border geometry and its defects so that it is virtually impossible to know what the local inclination angle of the magnetic field is. To render the problem tractable to analysis we resort to the following compromise: we still consider an infinitely wide and long layer of fluid and assume that the applied field is uniform, but we allow its arbitrary inclination with respect to the plane of the layer. Effectively, this adds two field direction angles to the standard problem's parameter list, see § 2.

Since ferrofluids do not retain magnetisation in the absence of an externally applied magnetic field they are sometimes classified as superparamagnets rather than ferromagnets (Albrecht *et al.* 1997). The next motivating factor for our current study is to demonstrate that such a terminology might be misleading if used blindly. We will show that even though the governing equations used to describe the behaviour of ferrofluids (see § 2) are indeed similar to those typically used for natural paramagnetic fluids such as oxygen (e.g. Ageikin 1950; Huang, Edwards & Gray 1997), flow instability patterns predicted using these equations in ferrofluids are qualitatively different from those found in paramagnetic fluids. We will show in § 4 that this distinction is brought about by a nonlinearity of the magnetic field inside a layer of ferrofluid, which is caused by a field inclination and a much stronger degree of ferrofluid magnetisation compared to that of paramagnetic fluids. This in turn leads to another methodological motivation of our current study: in contrast to paramagnetic fluids the flow stability characteristics of ferrofluids depend sensitively on the actual values of their magnetic susceptibilities, which vary widely with the magnitude of the applied field. Therefore special care should be taken when comparing computational and experimental results for ferrofluids to make sure that the analysis has been performed for fluid properties that vary in a way consistent with experimental conditions. This aspect of theoretical ferrofluid research has received insufficient attention in the previously reported studies and will be detailed in § 3. Remarkably, in contrast to the previous studies of magnetoconvection arising in a normal field (Finlayson 1970; Suslov 2008) we will show that the magnitude of the applied inclined magnetic field becomes an additional governing parameter of the problem.

Prior to proceeding with presenting our results we should stress that ferrofluids are complex multi-component colloidal systems and treating them as monofluids with spatially uniform properties cannot be justified in general. There is a growing body of evidence that effects such as gravitational sedimentation (Bozhko & Tynjala 2005; Bozhko *et al.* 2013) and thermophoresis (Völker & Odenbach 2003; Lange 2004; Ryskin & Pleiner 2004, 2007) of magnetic nano-particles as well as magnetoviscosity (e.g. Bashtovoy *et al.* 1988; Odenbach & Raj 2000; Odenbach 2002*a*,*b*, 2004; Odenbach & Müller 2005; Pop & Odenbach 2006; Engler, Borin & Odenbach 2009) can significantly affect experimentally observed ferrofluid flows. The detailed set of specific assumptions and physical conditions under which the governing equations considered in § 2 are expected to be accurate has been discussed in Suslov *et al.* (2012) and will be justified in §§ 2–4. Here we just state that we assume that the concentration of the magnetic phase remains uniform in the current study and therefore we will only investigate the influence of the thermal and magnetic fields on the flow structure. Such a simplified approach appears to be reasonable, at least

in the initial study, since the time scale for establishing thermosolutal gradients is significantly longer than that of the development of a thermomagnetic instability, and sedimentation effects are not present due to the lack of gravity.

The rest of the paper is organised as follows. The linearised perturbation equations are given in § 5 and their Squire-transformed form is interpreted in § 6. Their numerical solutions, the values of the determined critical parameters and a physical interpretation based on perturbation energy considerations are presented in § 7. Concluding remarks are given in § 8.

2. Problem formulation and governing equations

We will follow the major steps of the analysis presented in Finlayson (1970) and Suslov (2008). Namely, a linear flow stability analysis will be used to shed light on the physical mechanisms of the observed convection and to provide parametric guidance for further quantitative experimental study of fully nonlinear convection states driven by complex mechanisms in thin layers of ferro-colloids.

Consider a layer of a ferromagnetic fluid that fills the gap between two infinitely long and wide parallel non-magnetic plates as shown in figure 1. The plates are separated by the distance $2d$ and are maintained at constant different temperatures $T_* \pm \Theta$. An external uniform magnetic field, $\boldsymbol{H}^e = (H^e_x, H^e_y, H^e_z)$ such that $|\boldsymbol{H}^e| = H^e$, where $H^e_x = H^e \cos\delta$, $H^e_y = H^e \sin\delta \cos\gamma$ and $H^e_z = H^e \sin\delta \sin\gamma$, is applied at an arbitrary inclination to the layer. This field causes an internal magnetic field $\boldsymbol{H}$ such that $|\boldsymbol{H}| = H$ within the layer. The external field induces fluid magnetisation $\boldsymbol{M}$ such that $|\boldsymbol{M}| = M$, which is assumed to be co-directed with the internal magnetic field: $\boldsymbol{M} = \chi_* \boldsymbol{H}$, where χ_* is the integral magnetic susceptibility of the fluid. As discussed, for example, in Odenbach (2004) and references therein this is true if the magnetic particle size does not exceed $d_p \sim 13$ nm (the estimations based on the experimental data, see § 3, show that for the fluid used in the cited experiments the average value of d_p satisfies this condition). In this case the ratio of the Brownian particle magnetisation relaxation time $\tau_B = (4\pi d_p^3 \eta_*)/(k_B T)$, where $k_B = 1.38 \times 10^{-23}$ J K^{-1} is the Boltzmann constant, to the viscous time $\tau_v = \rho_* d^2/\eta_*$ characterising the macroflow development is $\tau_B/\tau_v \sim 10^{-5}$. Here, ρ_* is the fluid density and η_* is the dynamic viscosity. Thus it is safe to assume that the orientation of the magnetic moments of individual particles, and thus of the fluid magnetisation, follows the direction of a local magnetic field. The orientation of magnetic particle aggregates, however, can in principle be affected by the mechanical torque due to the local shear of the flow so that they can misalign with the local magnetic field. Yet the experiments reported in Odenbach & Müller (2005) show that such a misalignment only becomes noticeable for shear rates exceeding 15 s^{-1} while the shear rate for typical convection flows that are of interest here are of the order of 0.1 s^{-1} or even smaller. Therefore the misalignment of the magnetisation and magnetic field vectors can be safely neglected. We also assume that the fluid magnetisation depends only on magnetic field and temperature, which is the case when the concentration of magnetic particles remains uniform in experiments (we do not consider gravitational sedimentation, thermo- or magneto-phoresis of solid particles).

We choose the right-hand system of coordinates (x, y, z) with the origin in the mid-plane of the layer in such a way that the plates are located at $x = \pm d$ and the y and z axes are parallel to the plates. Assuming that the temperature difference 2Θ between the walls is sufficiently small, we adopt the Boussinesq approximation of the

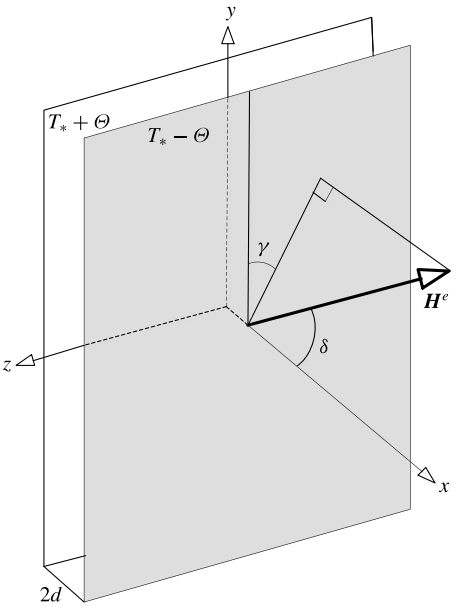

FIGURE 1. Sketch of the problem geometry. The vector of external magnetic field, $\boldsymbol{H}^e$, forms angles δ and γ with the coordinate axes.

continuity, Navier–Stokes and thermal energy equations, which are complemented with Maxwell's equations for the magnetic field:

$$\boldsymbol{\nabla} \cdot \boldsymbol{v} = 0, \tag{2.1}$$

$$\rho_* \frac{\partial \boldsymbol{v}}{\partial t} + \rho_* \boldsymbol{v} \cdot \boldsymbol{\nabla} \boldsymbol{v} = -\boldsymbol{\nabla} p + \eta_* \nabla^2 \boldsymbol{v} + \mu_0 M \boldsymbol{\nabla} H, \tag{2.2}$$

$$\frac{\partial T}{\partial t} + \boldsymbol{v} \cdot \boldsymbol{\nabla} T = \kappa_* \nabla^2 T, \tag{2.3}$$

$$\boldsymbol{\nabla} \times \boldsymbol{H} = 0, \quad \boldsymbol{\nabla} \cdot \boldsymbol{B} = 0, \tag{2.4a,b}$$

where

$$\boldsymbol{B} = \mu_0 (\boldsymbol{M} + \boldsymbol{H}), \quad \boldsymbol{M} = \frac{M(H, T)}{H} \boldsymbol{H}. \tag{2.5a,b}$$

In the above equations $\boldsymbol{v}$ is the velocity vector with the respective components (u, v, w) in the x, y and z directions, t is time, T is the temperature, p is the pressure, $\boldsymbol{B}$ is the magnetic flux density, κ_* is the thermal diffusivity of the fluid, and $\mu_0 = 4\pi \times 10^{-7}$ H m^{-1} is the magnetic constant. The subscript $*$ denotes the values of the fluid properties evaluated at the reference temperature T_* and reference internal magnetic field H_* (to be defined in § 4). In writing (2.2) we assume that the fluid remains Newtonian. It has been found in experiments of Bogatyrev & Gilev (1984) that this is a reasonable approximation for fluids with the concentration of solid phase not exceeding $f = 0.1$. The more recent measurements (however with different fluids) reviewed in Odenbach (2002*b*, chap. 4) have indicated that ferrofluids placed in a magnetic field can also behave as Bingham fluids with a non-zero yield stress that

increases approximately quadratically with the applied magnetic field. However the yield-stress magnitude remains very small for the field strength range relevant to the current study so that the Newtonian fluid approximation is well justified here.

As shown by numerous studies cited in § 1 the viscosity of concentrated ferrofluids depends on the applied magnetic field and the local flow shear that influence the concentration of aggregates formed as a result of a dipole interaction between magnetised particles. In general, both the average and local values of viscosity can vary. Even though many experiments aiming at quantifying such a dependence have been reported in the literature (e.g. Odenbach 2002*a*; Odenbach & Müller 2005; Pop & Odenbach 2006), the data collected in these experiments cannot be used directly to model flows in geometries and conditions that are significantly different from those of rheological experiments. Fortunately, in our study the reference layer-average fluid viscosity only enters the non-dimensional governing equations in combination with other fluid properties, forming the magnetic Rayleigh number (see § 3). We allow its value to vary over a wide range, which effectively includes all experimental conditions even though the exact value of magnetoviscosity remains unknown. The unknown variation of the local viscosity and other fluid properties subject to the action of the locally varying magnetic field and shear presents a more daunting problem. It is well known (e.g. Suslov & Paolucci 1995*a*,*b*) that, if sufficiently large, such a variation can strongly influence the structure of the flow and its stability. Yet to make analytical progress in the absence of a quantitative rheological model we are forced to neglect these spatial variations of fluid properties in (2.2). This is consistent with a widely used Boussinesq thermal approximation adapted for magnetic fluids (Bashtovoy *et al.* 1988) and is expected to be reasonable if the temperature and magnetic field variation across the layer remain small. The qualitative agreement between the computational results and the experimental observations reported in our previous work (Suslov *et al.* 2012) indicates that indeed such a simplification preserves sufficient accuracy of the model and makes it tractable. We provide a further discussion and a quantitative justification of this simplification in §§ 3 and 4.

The last term in (2.2) represents a ponderomotive (Kelvin) force that acts on a magnetised fluid in a non-uniform magnetic field, driving it toward regions with a stronger magnetic field as discussed in Bashtovoy *et al.* (1988). In order to close the problem, a magnetic equation of state is required, which is assumed to be in the simplest linear form valid for small temperature and field variations within the layer,

$$M = M_* + \chi\,\Delta H - K\Delta T, \quad \Delta H \equiv H - H_*, \quad \Delta T \equiv T - T_*. \tag{2.6a–c}$$

Here H_* and $M_* = \chi_* H_*$ are the magnitude of the magnetic field and the magnetisation at the location with temperature T_*, $\chi = \partial M/\partial H|_{(H_*,T_*)}$ is the differential magnetic susceptibility and $K = \partial M/\partial T|_{(H_*,T_*)}$ is the pyromagnetic coefficient. Using (2.6) we rewrite (2.5) as

$$\boldsymbol{M} = \frac{\chi H + (\chi_* - \chi)H_* - K\Delta T}{H}\boldsymbol{H}. \tag{2.7}$$

Subsequently, eliminating the magnetisation in favour of the magnetic field, we obtain from (2.4*b*)

$$(1+\chi)\nabla\cdot\boldsymbol{H} + \frac{(\chi_* - \chi)H_* - K\Delta T}{H}(\nabla\cdot\boldsymbol{H} - \nabla H\cdot\boldsymbol{e}) - K\nabla T\cdot\boldsymbol{e} = 0, \tag{2.8}$$

where $\boldsymbol{e} = (e_1, e_2, e_3) \equiv \boldsymbol{H}/H$ is the unit vector in the direction of the magnetic field. This equation shows that thermomagnetic coupling occurs mostly when the magnetic field and the temperature gradient have components in the same direction.

It is convenient to redefine pressure p entering the momentum equation (2.2) so that it includes both a hydrostatic component and a Kelvin force potential (see also Odenbach 2002*a*, pp. 86, 87). In order to do this we use (2.6) to write

$$\begin{aligned}\mu_0 M \nabla H &= \mu_0[M_* + \chi\Delta H - K\Delta T]\nabla H \\ &= \mu_0 \nabla\left[M_* H + \tfrac{1}{2}\chi\Delta H^2\right] - \mu_0 K \Delta T \nabla H. \end{aligned} \tag{2.9}$$

We will demonstrate in § 7.4 that only the non-potential component

$$F_K = -\mu_0 K \Delta T \nabla H \tag{2.10}$$

of the Kelvin force can lead to the destabilisation of a static mechanical equilibrium and result in magnetoconvection. Upon introducing the modified pressure

$$P = p - \mu_0\left[M_* H + \tfrac{1}{2}\chi\Delta H^2\right], \tag{2.11}$$

(2.2) is written as

$$\rho_* \frac{\partial \boldsymbol{v}}{\partial t} + \rho_* \boldsymbol{v}\cdot\nabla\boldsymbol{v} = -\nabla P + \eta_* \nabla^2 \boldsymbol{v} - \mu_0 K \Delta T \nabla H. \tag{2.12}$$

We impose the standard no-slip/no-penetration and thermal boundary conditions

$$\boldsymbol{v} = \boldsymbol{0}, \quad \Delta T = \pm\Theta \quad \text{at } x = \mp d \tag{2.13a,b}$$

for velocity and temperature, respectively. The magnetic boundary conditions are

$$(\boldsymbol{H}^e - \boldsymbol{H})\times\boldsymbol{n} = \boldsymbol{0}, \quad (\boldsymbol{B}^e - \boldsymbol{B})\cdot\boldsymbol{n} = 0 \quad \text{at } x = \pm d, \tag{2.14a,b}$$

where superscript e denotes fields outside the layer and $\boldsymbol{n} = (1, 0, 0)$ is the normal vector to the walls. Using (2.8), condition (2.14*b*) is rewritten as

$$[((1+\chi)H + (\chi_* - \chi)H_* \pm K\Theta)\,\boldsymbol{e} - \boldsymbol{H}^e]\cdot\boldsymbol{n} = 0 \quad \text{at } x = \pm d. \tag{2.15}$$

3. Non-dimensionalisation and problem parameters

The governing equations and boundary conditions are non-dimensionalised using

$$(x, y, z) = d(x', y', z'), \quad \boldsymbol{v} = \frac{\kappa_*}{d}\boldsymbol{v}', \quad t = \frac{d^2}{\kappa_*}t', \quad P = \frac{\rho_*\kappa_*^2}{d^2}P', \quad \Delta T = \Theta\theta', \tag{3.1a–e}$$

$$\boldsymbol{H} = \frac{K\Theta}{1+\chi}\boldsymbol{H}', \quad H = \frac{K\Theta}{1+\chi}H', \quad \boldsymbol{M} = \frac{K\Theta}{1+\chi}\boldsymbol{M}', \quad M = \frac{K\Theta}{1+\chi}M'. \tag{3.1f–i}$$

Then omitting primes for simplicity of notation, we obtain

$$\nabla\cdot\boldsymbol{v} = 0, \tag{3.2}$$

$$\frac{\partial\boldsymbol{v}}{\partial t} + \boldsymbol{v}\cdot\nabla\boldsymbol{v} = -\nabla P + Pr\nabla^2\boldsymbol{v} - Ra_m Pr\theta\nabla H, \tag{3.3}$$

$$\frac{\partial\theta}{\partial t}+\boldsymbol{v}\cdot\boldsymbol{\nabla}\theta=\nabla^2\theta, \tag{3.4}$$

$$\boldsymbol{\nabla}\times\boldsymbol{H}=\boldsymbol{0}, \tag{3.5}$$

$$(1+\chi)(\boldsymbol{\nabla}\cdot\boldsymbol{H}-\boldsymbol{\nabla}\theta\cdot\boldsymbol{e})+\frac{(\chi_*-\chi)N-(1+\chi)\theta}{H}(\boldsymbol{\nabla}\cdot\boldsymbol{H}-\boldsymbol{\nabla}H\cdot\boldsymbol{e})=0, \tag{3.6}$$

$$\boldsymbol{M}=[\chi H+(\chi_*-\chi)N-(1+\chi)\theta]\boldsymbol{e}, \tag{3.7}$$

with the boundary conditions

$$[((1+\chi)(H\pm1)+(\chi_*-\chi)N)\,\boldsymbol{e}-\boldsymbol{H}^e]\cdot\boldsymbol{n}=0, \tag{3.8}$$

$$\boldsymbol{v}=\boldsymbol{0},\quad \theta=\mp1\quad\text{at } x=\pm1. \tag{3.9}$$

The dimensionless parameters appearing in the problem are

$$Ra_m=\frac{\mu_0K^2\Theta^2d^2}{\eta_*\kappa_*(1+\chi)},\quad Pr=\frac{\eta_*}{\rho_*\kappa_*},\quad N=\frac{H_*(1+\chi)}{K\Theta}. \tag{3.10a–c}$$

The magnetic Rayleigh number Ra_m characterises the importance of magnetic forces, Prandtl number Pr characterises the ratio of viscous and thermal diffusion transport, and parameter N represents the non-dimensional magnetic field at the reference location.

Typical parameter values that are reported in the recent experiments (Suslov *et al.* 2012; Bozhko *et al.* 2013) are listed in table 1. Based on physical quantities listed in this table we estimate the value of Prandtl number Pr to be around 55 and use this for our computations. Note, however, that our previous results (Suslov 2008) for a normal field have been reported in terms of magnetic Grashof number for $Pr=130$. However, this does not prevent us from performing a meaningful comparison of the current and past results because in the case of pure magnetoconvection (in the absence of gravity) considered here the critical values of Ra_m are found to be invariant with respect to the values of Prandtl number. Thus for comparison with the previous results we simply use the relationship

$$Gr_m(Pr)=\frac{Ra_m}{Pr}, \tag{3.11}$$

where Ra_m is the invariant value reported in the current paper and Pr is the value of Prandtl number used elsewhere.

Among other important physical quantities characterising the field-dependent magnetic properties of the fluid are the differential and integral magnetic susceptibilities χ and χ_* and pyromagnetic coefficient K, which depend on the applied magnetic field and the temperature. The pyromagnetic coefficient K only enters the governing equations as a component of the non-dimensional groups (3.10) so that its exact value is not required for the current analysis, see a similar discussion of fluid viscosity in § 2. However we will see in § 4 that the magnitude of K (and thus of parameter N) can be conveniently used to distinguish between paramagnetic and ferromagnetic fluids. At the same time, the values of magnetic susceptibilities χ and χ_* are important problem parameters entering the governing equations directly. It is a common practice to estimate them from the Langevin magnetisation law

$$M_L(H)=M_\infty L(\xi),\quad L(\xi)=\coth\xi-\frac{1}{\xi},\quad \xi=\mu_0\pi\frac{M_sd_p^3H}{6k_BT}, \tag{3.12a–c}$$

Notation	Parameter	Typical value
f	Volume concentration of magnetic phase	0.1
ρ_*	Density	1.44×10^3 kg m^{-3}
β_*	Coefficient of thermal expansion	7.7×10^{-4} K^{-1}
κ_*	Thermal diffusivity	1×10^{-8} m^2 s^{-1}
η_*	Dynamic viscosity in absence of magnetic field	7.66×10^{-3} kg m^{-1} s^{-1}
H^e	External magnetic field	0–3.5×10^4 A m^{-1}
T_*	Average (reference) temperature in the layer	293 K
2Θ	Temperature difference between the walls	1–30 K
$2d$	Distance between the walls	6 mm

TABLE 1. The typical values of experimental parameters and properties of the ferrofluid manufactured in the Scientific Laboratory of Practical Ferromagnetic Fluids, Ivanovo, Russia under Technical Conditions 229-001-02068195-2002 and used in experiments reported in Suslov *et al.* (2012) and Bozhko *et al.* (2013).

where M_∞ is the experimentally measured saturation magnetisation of the fluid, $L(\xi)$ is Langevin's function and ξ is Langevin's parameter. Here M_s is the saturation magnetisation of a magnetic phase at a given temperature and d_p^3 is the average cube of the diameter of a magnetised core of solid particles. Due to the Curie effect (demagnetisation of a ferromagnetic fluid with increasing temperature) and thermal expansion of the carrier fluid, the saturation magnetisation of magnetic material and ferrofluid vary as

$$M_s = M_{s*}\frac{1-\beta_2 T^2}{1-\beta_2 T_*^2}, \tag{3.13}$$

$$M_\infty = M_{\infty *}\frac{1-\beta_2 T^2}{1-\beta_2 T_*^2}(1-\beta_*(1-f)(T-T_*)), \tag{3.14}$$

where β_* is the coefficient of thermal expansion of the carrier fluid, β_2 is the Curie coefficient and f is the volume fraction of the magnetic phase. In this study, magnetite particles with $M_{s*} = 480$ kA m^{-1} and $\beta_2 = 8 \times 10^{-7}$ K^{-2} at reference temperature $T_* = 293$ K are considered, which correspond to the experimental fluids referred to in the previous publications (Suslov 2008; Suslov *et al.* 2012; Bozhko *et al.* 2013). The fluid saturation magnetisation measured at $T_* = 293$ K was $M_{\infty *} = 43$ kA m^{-1}.

However, both experimental measurements and molecular dynamics simulations show that the magnetisation law of a realistic ferrofluid deviates significantly from the Langevin dependence. The main reason for this is that Langevin's law assumes no inter-particle interactions, which is not the case for experimental fluids with magnetic phase concentration as high as $f = 0.1$. A comprehensive review of this issue is given in Ivanov *et al.* (2007). There the authors showed that a significant improvement of the accuracy of the magnetisation law for a ferrofluid is obtained via the use of the so-called second-order modified mean field (MMF2) model that is essentially a two-term expansion of the Weiss mean field model (Weiss 1907; Tsebers 1982). It is obtained by replacing the Langevin parameter ξ with

$$\bar{\xi} = \mu_0 \pi \frac{M_s d_p^3 \bar{H}}{6 k_B T}, \quad \bar{H} = H + \frac{1}{3} M_L(H)\left(1 + \frac{1}{48}\frac{\mathrm{d}M_L(H)}{\mathrm{d}H}\right). \tag{3.15a,b}$$

Here $\bar{H}$ is the effective magnetic field that takes into account mean magnetic interactions between particles in a concentrated magnetic fluid.

The only physical quantity that remains unknown in the above formulae is the average cube of the diameter of magnetised particle cores. This quantity depends strongly on the (unknown) size dispersion of nano-particles and their aggregates present in the fluid. Thus d_p^3 was determined by matching the predictions of the initial differential magnetic susceptibility $\lim_{H\to 0}\chi(H)$ of the fluid with its experimentally determined value $\chi = 3$ (Pshenichnikov 2007; Lebedev & Lysenko 2011). It turned out that the MMF2 model produces this value if $d_p^3 \approx 1.64\times 10^{-24}$ m^3.

Even though the MMF2 model is shown to produce accurate values for magnetic properties of a ferrofluid, it requires the value of a local magnetic field H as an input. However, this quantity depends on the geometry of the problem considered. For example, it was shown in Suslov (2008) that when an external magnetic field H^e is applied perpendicularly to an infinite differentially heated layer of a ferrofluid bounded by parallel non-magnetic plates the internal magnetic field in the mid-plane of the layer is $H_* = H^e/(1+\chi_*)$. The values of H_* and the corresponding fluid magnetisation M_* are shown in figure 2(*c*) for the experimental range of external magnetic field $0 \leqslant H^e \leqslant 35$ kA m^{-1}. If the magnetic field is applied obliquely then the relationship between the external and internal fields becomes much more complicated, see § 4. However, in this study we are mostly interested in the qualitative behaviour of the system for relatively small field inclination angles $0^\circ \leqslant \delta \leqslant 15^\circ$. Therefore the data presented in figure 2 for $\delta = 0^\circ$ will suffice for parameter estimation purposes.

The comparison of relevant quantities obtained using Langevin and MMF2 models given in figure 2 demonstrates that Langevin's law systematically underestimates the values of the magnetic susceptibilities and the pyromagnetic coefficient. Thus we use MMF2 curves to choose the range of parameters for which the numerical results will be presented. As seen from figure 2(*a*) the values of magnetic susceptibilities change over the range of the applied magnetic field from $(\chi,\ \chi_*) = (3,\ 3)$ to just below $(\chi,\ \chi_*) = (1.5,\ 2.5)$. Thus we will report the numerical results for these two pairs of values. We also note that the previous numerical results are available (see Suslov 2008) for $(\chi,\ \chi_*) = (5,\ 5)$. Therefore, for comparison purposes we will also perform computations for this pair of parameters as well as for $(\chi,\ \chi_*) = (3,\ 5)$. Note that as discussed in Finlayson (1970) and Suslov (2008), $\chi = \chi_*$ along the linear segment of the magnetisation curve. However, $\chi < \chi_*$ when the fluid's magnetisation approaches saturation. Therefore, by choosing different values of the differential and integral magnetic susceptibilities, we investigate the effect of nonlinearity of the magnetisation law on flow stability.

As mentioned previously, the value of the pyromagnetic coefficient K enters the definition of magnetic Rayleigh number. In this study the data from figure 2(*b*) are not used to limit the computational range of Ra_m but, rather, are presented here to enable the design of chambers for future experiments where the thickness of the gap between the walls will need to be chosen so that it results in the values of parameters close to critical ones reported in this study.

Figure 2(*d*) shows the values of the normally applied non-dimensional external magnetic field $H^{e\prime}$ and the corresponding reference internal magnetic field $N_0 = N|_{\delta=0^\circ}$ (here we use a prime to denote a non-dimensional external field in figure 2(*d*) and to distinguish it from the dimensional external field H^e; however, for simplicity of notation we will use H^e to denote the non-dimensional field in the subsequent text). These parameters are not independent. It has been shown in Suslov (2008) that

$$H^{e\prime} = (1+\chi_*)N_0 \tag{3.16}$$

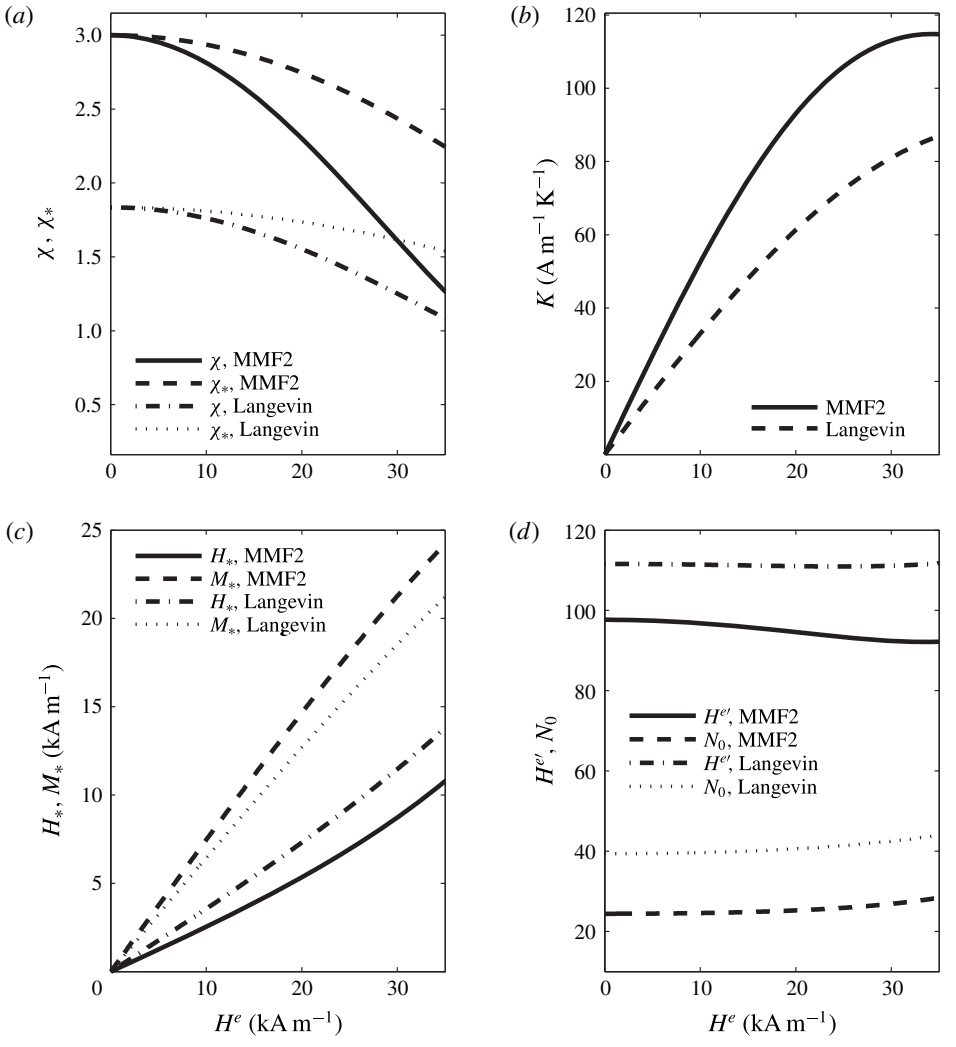

FIGURE 2. The comparison of magnetic fluid properties defined using Langevin's law and the MMF2 model for $\delta = 0°$ and $T_* = 293$ K ($\Theta = 7.5$ K is chosen in (d)).

when $\delta = 0°$. It is also known that neither of these two parameters affects the stability characteristics of the flow when the magnetic field is perpendicular to the layer if the magnetisation law is linear (Finlayson 1970; Suslov 2008). However, when the nonlinearity of magnetisation is taken into account and when the field is applied obliquely the role of these parameters becomes non-trivial. It will be demonstrated in § 4 that whenever $\delta \neq 0°$ the magnetic field lines within the layer curve. This curvature will be shown to be responsible for a qualitative change in the behaviour of the perturbation fields compared to that observed when $\delta = 0°$. The relationship between parameters N and $H^{e\prime}$ for a general oblique field cannot be given explicitly (apart from some limiting cases discussed in § 4) yet it is still well approximated by (3.16). It is convenient to use N_0 for expressing solutions for magnetic field within the layer symbolically and $H^{e\prime}$ for parameterising the numerical stability results. Figure 2(d) shows that for all experimentally relevant conditions the value of $H^{e\prime}$

(and N_0) remains large and close to constant for fixed temperature difference 2Θ between the walls. Therefore we choose $H^{e\prime} = 100$ in our computations, which is close to the values achieved in experiments. Our calculations show that the numerical stability results become almost independent of $H^{e\prime}$ when its value exceeds 40 (this is the case when the temperature difference between the walls does not exceed about 30 K, which is the experimental maximum). We also present some selected results for $H^{e\prime} = 10$. This would correspond to the temperature difference ΔT between the walls of more than 100°, which is experimentally unachievable with the fluids used in the referenced experiments. However, such a value of $H^{e\prime}$ could be realistic for a stronger magnetisable fluid (e.g. one with a higher concentration of magnetic particles and thus with a larger pyromagnetic coefficient). Therefore, we present the numerical results for $H^{e\prime} = 10$ as well, which allows us to see more clearly the peculiar qualitative effects brought about by the inclination of a magnetic field and the resulting curvature of magnetic field lines (see figure 5*a,c* below).

4. Basic flow

We look for steady motionless solutions of (3.2)–(3.9) in the form

$$\boldsymbol{v}_0 = \boldsymbol{0}, \quad \theta_0 = \theta_0(x), \quad P_0 = P_0(x), \quad \boldsymbol{H}_0 = (H_{x0}(x), H_{y0}(x), H_{z0}(x)). \tag{4.1a–d}$$

They should satisfy

$$\mathrm{D}P_0 = -Ra_m Pr\theta_0 e_{10}\mathrm{D}H_{x0}, \quad \mathrm{D}^2\theta_0 = 0, \tag{4.2a,b}$$

$$\mathrm{D}\left(\left(1+\frac{M_0}{H_0}\right)H_{x0}\right) = 0, \tag{4.3}$$

$$\mathrm{D}H_{y0} = 0, \quad \mathrm{D}H_{z0} = 0, \tag{4.4a,b}$$

and the boundary conditions

$$\theta_0 = \pm 1, \quad H_{y0} = H_y^e, \quad H_{z0} = H_z^e, \tag{4.5a–c}$$

$$\left(1+\frac{M_0}{H_0}\right)H_{x0} = H_x^e \quad \text{at } x = \mp 1, \tag{4.6}$$

where $H_0 \equiv \sqrt{H_{x0}^2 + H_{y0}^2 + H_{z0}^2}$, $M_0 \equiv \sqrt{M_{x0}^2 + M_{y0}^2 + M_{z0}^2}$ and $\mathrm{D} \equiv \mathrm{d}/\mathrm{d}x$. Upon introducing the unit vector $\boldsymbol{e}_0(x) \equiv (e_{10}(x), e_{20}(x), e_{30}(x)) = \left(H_{x0}/H_0, H_{y0}/H_0, H_{z0}/H_0\right)$ in the direction of the magnetic field the basic flow solutions of (4.2) are written as

$$\theta_0 = -x \quad \text{and} \quad P_0 = Ra_m Pr \int_0^x \bar{x} e_{10}\mathrm{D}H_{x0}\,\mathrm{d}\bar{x} + C, \tag{4.7}$$

where C is an arbitrary constant. Equations (4.4) along with boundary conditions (4.5) result in expressions for tangential components of the magnetic field that are constant inside the fluid layer, $H_{y0}(x) = H_y^e$ and $H_{z0}(x) = H_z^e$. In view of (3.7) and (4.6), equation(4.3) is integrated to obtain a nonlinear algebraic equation for the x-component of the unperturbed magnetic field

$$((1+\chi)(H_0 - \theta_0) + (\chi_* - \chi)N)\,H_{x0} = H_x^e H_0. \tag{4.8}$$

It is known (e.g. Suslov 2008) that for a perpendicular field when $\boldsymbol{e}_0 = (1, 0, 0)$ the basic flow component of the magnetic field in the x direction across the layer is given by $H_{x0} = N_0 - x$, where N_0 is defined by (3.16). However, when the external field is applied obliquely a nonlinear equation (4.8) does not have a closed-form solution and

has to be solved numerically. Yet by evaluating this equation at the reference position $x = 0$ we obtain exact expressions for the magnetic field and its x component there:

$$H_{x0}(0) = N_0 \cos\delta, \quad N \equiv H_0(0) = N_0 \cos\delta \sqrt{1 + (1+\chi_*)^2 \tan^2\delta}. \tag{4.9a,b}$$

It follows from (4.9) and (3.16) that the magnetic field in the mid-plane of the layer monotonically increases from N_0 for a normal field to H^e when the applied field is tangential to the layer.

Taking into account that $N_0 \gg x$ as discussed in § 3 the solution of (4.8) can also be written asymptotically as

$$\frac{H^a_{x0}}{N_0 \cos\delta} = 1 - \frac{1+\chi}{(1+\chi_*)^3 \sin^2\delta + (1+\chi)\cos^2\delta} \frac{N}{N_0} \frac{x}{N_0} + \sin^2\delta \frac{(1+\chi)^2(1+\chi_*)^3 \left(\dfrac{N^2}{N_0^2} + \dfrac{1}{2} \dfrac{\chi_* - \chi}{1+\chi_*} \cos^2\delta \right)}{((1+\chi_*)^3 \sin^2\delta + (1+\chi)\cos^2\delta)^3} \frac{x^2}{N_0^2} + o\left(\frac{x^2}{N_0^2}\right). \tag{4.10}$$

A similar asymptotic approach was used in Hennenberg *et al.* (2006) to determine the approximate expression for the magnetic field in a layer of magnetic fluid subject to longitudinal temperature gradient (in contrast to the transverse gradient considered here).

If the magnetisation law is linear, that is if $\chi = \chi_*$, the above expression simplifies to

$$\frac{H^a_{x0}}{N_0 \cos\delta} = 1 - \frac{x}{N} + (1+\chi)^2 \sin^2\delta \frac{N_0^2}{N^2} \frac{x^2}{N^2} + o\left(\frac{x^2}{N^2}\right). \tag{4.11}$$

The first two terms in the asymptotic solution (4.11) are equivalent to expression (9) given in Huang *et al.* (1997) for a magnetic field in a layer of paramagnetic fluid with $\chi = \chi_* \ll 1$. However, the nonlinearity of the magnetic field in the layer was fully neglected in Huang *et al.* (1997). As seen from expressions (4.10) and (4.11) this is only true when $N_0 \to \infty$, that is when pyromagnetic coefficient $K \to 0$, see definition (3.10). This is shown to be a good approximation in the case of paramagnetic fluids (Huang *et al.* 1997); however, K is large in the current problem, see figure 2(*b*). Therefore N_0 is finite and the nonlinearity of the magnetic field inside the layer of ferromagnetic fluid cannot be ignored. This is confirmed by fully nonlinear numerical solutions for the magnetic field shown for the finite values of $\chi = \chi_* = 3$ in figure 3. The degree of nonlinearity increases with decreasing value of the applied magnetic field provided that the value of the pyromagnetic coefficient does not vary significantly. Yet the three-term asymptotic solution (4.10) remains robust, providing accuracy within 1–2 % of the numerically computed values in all regimes considered.

Importantly, figure 3 demonstrates that the relative deviation of the magnetic field within the layer from its average value cannot exceed $1/N_0$. Using the data presented in figure 2(*d*) one then concludes that the field varies within the layer by less than 4 %. This is a natural measure of the error that is introduced in the model considered by assuming that the field-dependent fluid properties remain constant in (2.2).

Once the magnetic field within the layer is determined the unperturbed fluid magnetisation is computed using

$$M_0 = \chi H_0 + (\chi_* - \chi)N - (1+\chi)\theta_0. \tag{4.12}$$

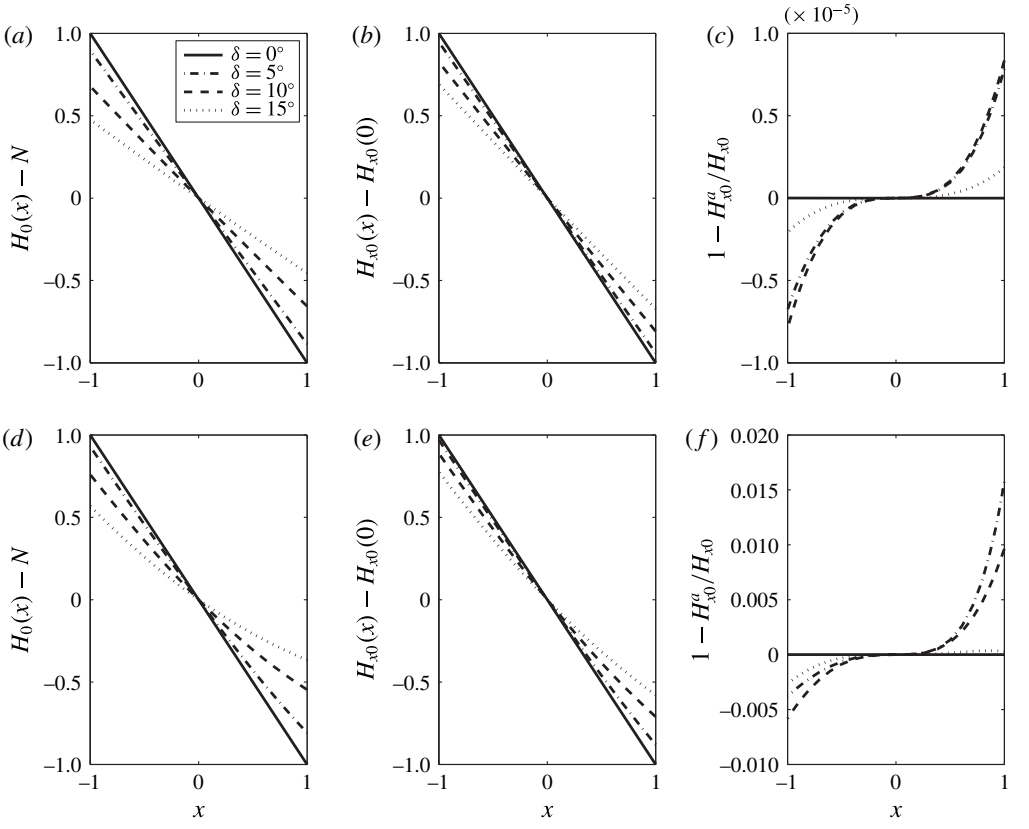

FIGURE 3. Numerical solution for the magnitude H_0 of the undisturbed magnetic field (*a,d*) and its cross-layer component H_{x0} (*b,e*), for $H^e = 100$ (*a,c*), $H^e = 10$ (*d,e*), $\chi = \chi_* = 3$ and various field inclination angles δ. (*c,e*) The corresponding relative error of the asymptotic solution (4.10).

Typical distributions of the magnetisation and magnetic pressure across the layer are shown in figure 4. Both figures 3 and 4 demonstrate that the field inclination leads to a noticeable difference between the magnitudes of the cross-layer components of magnetic and magnetisation fields and their full magnitudes. This difference is more pronounced near the cold wall, which introduces an asymmetry in basic flow fields that will be shown to influence the stability results qualitatively. The other observation is that the magnitude of the external magnetic field influences the fields inside the layer: weaker oblique external fields lead to a stronger nonlinearity of internal fields (compare the top and bottom rows in figures 3 and 4). The symmetry-breaking effect of the field inclination is also evident in the behaviour of the magnetic pressure P_0 shown in figure 4(*c,f*). As the field inclination angle increases, the pressure near the cold wall grows with respect to that near the hot wall. As will be discussed later this leads to the preferential shift of instability structures toward the hot wall, which introduces a further asymmetry and qualitative change in stability characteristics compared to the normal field case considered in Finlayson (1970) and Suslov (2008).

The behaviour of magnetic field lines inside a layer of ferrofluid is shown in figure 5(*a,c*). In contrast to the case of a normal field considered in Finlayson (1970) and Suslov (2008), the non-dimensional magnitude (relative to the fluid magnetisation)

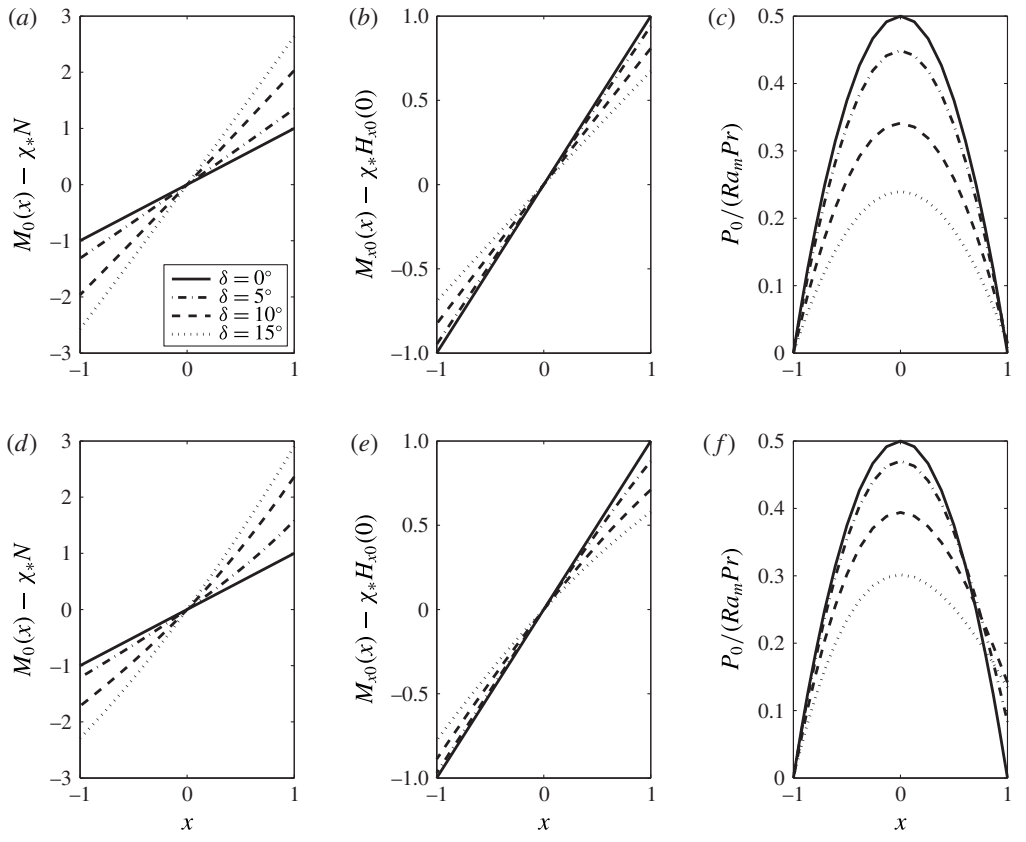

FIGURE 4. Numerical solution for the magnitude M_0 of the undisturbed fluid magnetisation (*a,d*), its cross-layer component M_{x0} (*b,e*) and magnetic pressure P_0 (*c,f*), for $H^e = 100$ (*a–c*), $H^e = 10$ (*d–f*), $\chi = \chi_* = 3$ and various field inclination angles δ.

of the obliquely applied field strongly affects the geometry of magnetic lines. The curvature of magnetic lines is especially pronounced in stronger magnetisable fluids (plot (*c*) as contrasted to plot (*a*)). This has a profound effect on the distribution of the normal non-potential component $F_{K0} = -\theta_0(\mathrm{d}H_0/\mathrm{d}x)$ of the non-dimensional Kelvin force, which can be viewed as a magnetic buoyancy force. It is shown in figure 5(*b,d*). Such a force is positive near the left wall and negative near the right wall, which corresponds to an inherently unstable situation when hot fluid near $x = -1$ is forced to flow toward the cold wall at $x = 1$ and vice versa. This situation is similar to an unstably stratified layer of a regular fluid heated from below in a downward gravitational field. Yet such similarity is complete only if the external magnetic field is normal to the layer. In this case, similar to its gravitational counterpart, the magnetic buoyancy is a linear function of the cross-layer coordinate x and its non-dimensional value is independent of the strength of the applied field, see dashed lines in figure 5(*b,d*). However, when an oblique field of the same magnitude is applied to the layer at least three qualitative differences arise due to the nonlinearity of the induced internal field. Firstly, the magnetic buoyancy force becomes more uniform across the layer so that the onset of thermomagnetic instability is expected to be delayed compared to the normal field situation. Secondly, the magnetic buoyancy

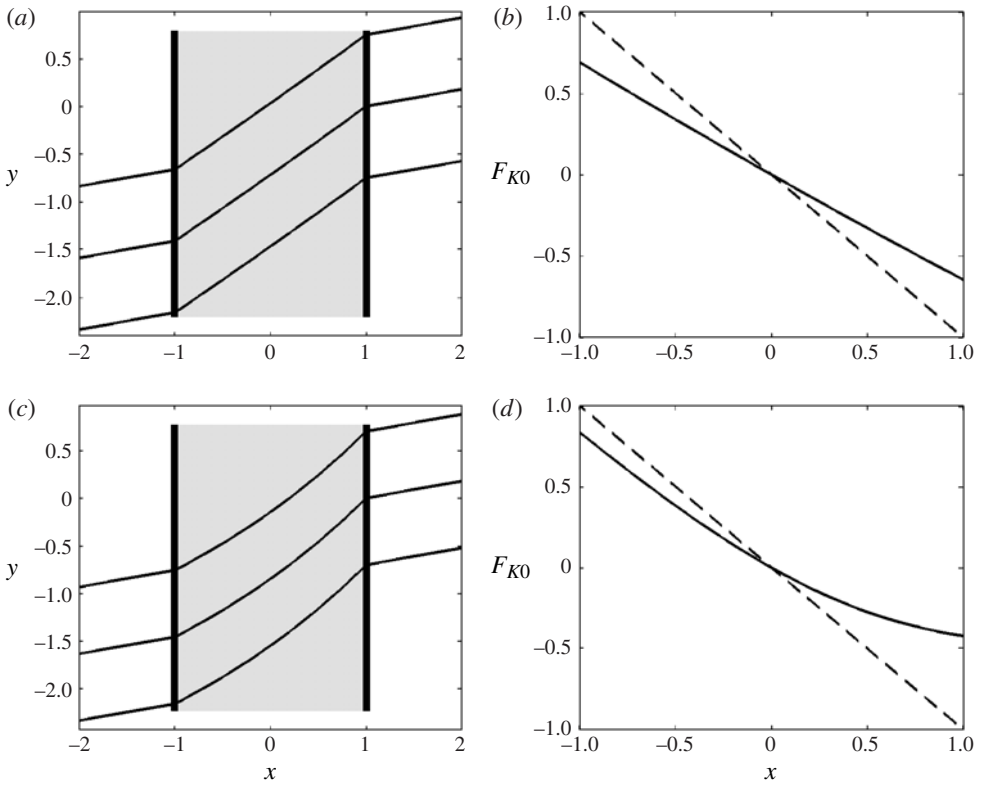

FIGURE 5. Refraction of magnetic lines (*a,c*) and the distribution of the Kelvin force (*b,d*) in a layer of magnetic fluid heated from the left for the field inclination angles $\delta = 10°$ (solid line), $\delta = 0°$ (dashed line), $\gamma = 0°$, $\chi = \chi_* = 3$, $H^e = 100$ (*a,b*) and $H^e = 10$ (*c,d*).

force becomes a function of the magnitude of the applied magnetic field. Thirdly, and most importantly, the nonlinearity of the internal magnetic field leads to the situation where the layer that is unstably stratified with respect to magnetic buoyancy is effectively reduced to a sublayer in the vicinity of the hot wall, see figure 5(*d*). Therefore, in contrast to the case of a normal field, the cross-layer symmetry of the instability structures that arise is broken. In the following sections we will establish and quantify the physical features of instability patterns that are brought about by the inclination of an external field and were not found in the previous studies reported in Finlayson (1970) and Suslov (2008).

5. Linearised perturbation equations

In order to investigate linear stability of the basic state discussed in § 4 with respect to infinitesimal disturbances that are assumed to be periodic in the y and z directions we consider a standard normalform representation of the perturbed quantities and write them as

$$\begin{aligned}(\boldsymbol{v}, P, \theta, \boldsymbol{H}, H, \boldsymbol{M}, M)\\ = (\boldsymbol{v}_0, P_0, \theta_0, \boldsymbol{H}_0, H_0, \boldsymbol{M}_0, M_0)\\ + [(\boldsymbol{v}_1(x), P_1(x), \theta_1(x), \boldsymbol{H}_1(x), H_1(x), \boldsymbol{M}_1(x), M_1(x))\mathrm{e}^{\sigma t + \mathrm{i}(\alpha y + \beta z)} + \text{c.c.}], \quad (5.1)\end{aligned}$$

where $\sigma = \sigma^R + \mathrm{i}\sigma^I$ is the complex amplification rate, α and β are real wavenumbers in the y and z directions, respectively, and c.c. denotes the complex conjugate of the expression in square brackets. To satisfy (3.5) identically, it is convenient to introduce a perturbation $\phi_1(x)\mathrm{e}^{\sigma t+\mathrm{i}(\alpha y+\beta z)}$ of the magnetic potential so that

$$\boldsymbol{H}_1 = [\mathrm{D}\phi_1, \mathrm{i}\alpha\phi_1, \mathrm{i}\beta\phi_1]^{\mathrm{T}}, \tag{5.2a}$$

$$H_1 = \boldsymbol{H}_1 \cdot \boldsymbol{e}_0 = e_{10}\mathrm{D}\phi_1 + \mathrm{i}(\alpha e_{20} + \beta e_{30})\phi_1, \tag{5.2b}$$

$$\boldsymbol{M}_1 = \chi \boldsymbol{H}_1 - (1+\chi)\theta_1\boldsymbol{e}_0 + \frac{(1+\chi)\theta_0 - (\chi_* - \chi)N}{H_0}(H_1\boldsymbol{e}_0 - \boldsymbol{H}_1), \tag{5.2c}$$

$$M_1 = \boldsymbol{M}_1 \cdot \boldsymbol{e}_0 = \chi H_1 - (1+\chi)\theta_1. \tag{5.2d}$$

The linearisation of (3.2)–(3.9) about the basic state leads to

$$0 = \mathrm{D}u_1 + \mathrm{i}(\alpha v_1 + \beta w_1), \tag{5.3}$$

$$\begin{aligned}
&\sigma u_1 + Pr(\alpha^2+\beta^2-\mathrm{D}^2)u_1 + \mathrm{D}P_1 + e_{10}Ra_mPr\mathrm{D}H_{x0}\,\theta_1 \\
&\quad + Ra_mPr\theta_0 e_{10}\mathrm{D}^2\phi_1 + Ra_mPr\theta_0\left(\mathrm{i}(\alpha e_{20}+\beta e_{30}) + (1-e_{10}^2)\frac{\mathrm{D}H_{x0}}{H_0}\right)\mathrm{D}\phi_1 \\
&\quad - \mathrm{i}Ra_mPr\theta_0 e_{10}(\alpha e_{20}+\beta e_{30})\frac{\mathrm{D}H_{x0}}{H_0}\phi_1 = 0,
\end{aligned} \tag{5.4}$$

$$\begin{aligned}
&\sigma v_1 + Pr(\alpha^2+\beta^2-\mathrm{D}^2)v_1 + \mathrm{i}\alpha P_1 \\
&\quad + \mathrm{i}\alpha Ra_mPr\theta_0 e_{10}\mathrm{D}\phi_1 - \alpha Ra_mPr\theta_0(\alpha e_{20}+\beta e_{30})\phi_1 = 0,
\end{aligned} \tag{5.5}$$

$$\begin{aligned}
&\sigma w_1 + Pr(\alpha^2+\beta^2-\mathrm{D}^2)w_1 + \mathrm{i}\beta P_1 \\
&\quad + \mathrm{i}\beta Ra_mPr\theta_0 e_{10}\mathrm{D}\phi_1 - \beta Ra_mPr\theta_0(\alpha e_{20}+\beta e_{30})\phi_1 = 0,
\end{aligned} \tag{5.6}$$

$$\sigma\theta_1 + \mathrm{D}\theta_0 u_1 + (\alpha^2+\beta^2-\mathrm{D}^2)\theta_1 = 0, \tag{5.7}$$

$$\begin{aligned}
0 = {} & (\mathrm{D}^2-\alpha^2-\beta^2)\phi_1 + (1-e_{10}^2)\left(\frac{\chi_*-\chi}{1+\chi}N - \theta_0\right)\frac{\mathrm{D}^2\phi_1}{H_0} \\
& - \left[e_{10}\left(\frac{\chi_*-\chi}{1+\chi}N-\theta_0\right)\left(2\mathrm{i}(\alpha e_{20}+\beta e_{30}) + 3(1-e_{10}^2)\frac{\mathrm{D}H_{x0}}{H_0}\right)\right. \\
& \left. + (1-e_{10}^2)\mathrm{D}\theta_0\right]\frac{\mathrm{D}\phi_1}{H_0} - \left[\left(\frac{\chi_*-\chi}{1+\chi}N-\theta_0\right)\right. \\
& \times \left(\alpha^2+\beta^2-(\alpha e_{20}+\beta e_{30})^2 + \mathrm{i}(\alpha e_{20}+\beta e_{30})(1-3e_{10}^2)\frac{\mathrm{D}H_{x0}}{H_0}\right) \\
& \left. - \mathrm{i}(\alpha e_{20}+\beta e_{30})e_{10}\mathrm{D}\theta_0\right]\frac{\phi_1}{H_0} \\
& - \left(\mathrm{i}(\alpha e_{20}+\beta e_{30}) + (1-e_{10}^2)\frac{\mathrm{D}H_{x0}}{H_0}\right)\theta_1 - e_{10}\mathrm{D}\theta_1.
\end{aligned} \tag{5.8}$$

The disturbance velocity and temperature fields are subject to standard homogeneous boundary conditions

$$u_1 = v_1 = w_1 = \theta_1 = 0 \quad \text{at } x = \pm 1. \tag{5.9}$$

A perturbation of a magnetic field within a fluid layer causes perturbation of the external magnetic field for non-magnetic boundaries as discussed in Finlayson (1970). If there are no induced currents outside the layer and a non-magnetic medium (air) fills the surrounding space, then the external magnetic field has a potential $\phi_1^e(x)\exp(\sigma t + \mathrm{i}\alpha y + \mathrm{i}\beta z)$, which, as follows from (2.4) and (2.5), satisfies Laplace's equation

$$(\mathrm{D}^2 - \alpha^2 - \beta^2)\phi_1^e = 0, \tag{5.10}$$

in the regions $x < -1$ and $x > 1$. A physically relevant bounded solution can be written as

$$\phi_1^e(x) = \begin{cases} A\exp\left(\sqrt{\alpha^2+\beta^2}x\right), & x < -1 \\ B\exp\left(-\sqrt{\alpha^2+\beta^2}x\right), & x > 1. \end{cases} \tag{5.11}$$

Upon taking into account (2.5), the linearisation of the magnetic boundary conditions (2.14) leads to

$$\begin{aligned} \mathrm{D}\phi_1^e \;=\; & \left(1+\chi+(1-e_{10}^2)\frac{(\chi_*-\chi)N\pm(1+\chi)}{H_0}\right)\mathrm{D}\phi_1 \\ & -\mathrm{i}e_{10}(\alpha e_{20}+\beta e_{30})\frac{(\chi_*-\chi)N\pm(1+\chi)}{H_0}\phi_1, \end{aligned} \tag{5.12}$$

$$\phi_1^e = \phi_1 \quad \text{at } x = \pm 1. \tag{5.13}$$

After eliminating A and B from (5.11) and (5.13) we obtain the boundary conditions for ϕ_1 at $x = \pm 1$:

$$\begin{aligned} & \left(1+\chi+(1-e_{10}^2)\frac{(\chi_*-\chi)N\pm(1+\chi)}{H_0}\right)\mathrm{D}\phi_1 \\ & \pm\sqrt{\alpha^2+\beta^2}\phi_1 - \mathrm{i}e_{10}(\alpha e_{20}+\beta e_{30})\frac{(\chi_*-\chi)N\pm(1+\chi)}{H_0}\phi_1 = 0. \end{aligned} \tag{5.14}$$

6. Squire's transformation

Upon using the generalised Squire's transformations

$$\left.\begin{gathered} (x,y,z) = (\tilde{x},\tilde{y},\tilde{z}), \quad \theta_0 = \tilde{\theta}_0, \quad H_{x0} = \tilde{H}_{x0}, \quad H_0 = \tilde{H}_0, \quad \sigma = \tilde{\sigma}, \quad \alpha^2+\beta^2 = \tilde{\alpha}^2, \\ \beta = \tilde{\beta}, \quad u_1 = \tilde{u}, \quad \alpha v_1 + \beta w_1 = \tilde{\alpha}\tilde{v}, \quad w_1 = \tilde{w}, \quad \theta_1 = \tilde{\theta}, \quad P_1 = \tilde{P}, \quad \phi_1 = \tilde{\phi}, \\ Ra_m = \widetilde{Ra}_m, \quad Pr = \widetilde{Pr}, \quad N = \tilde{N}, \quad \chi = \tilde{\chi}, \quad \chi_* = \tilde{\chi}_*, \\ e_{10} = \tilde{e}_{10}, \quad \alpha e_{20} + \beta e_{30} = \tilde{\alpha}\tilde{e}_{20}, \end{gathered}\right\} \tag{6.1}$$

(5.3)–(5.8) become

$$0 = \mathrm{D}\tilde{u} + \mathrm{i}\tilde{\alpha}\tilde{v}, \tag{6.2}$$

$$\begin{aligned} & \tilde{\sigma}\tilde{u} + \widetilde{Pr}(\tilde{\alpha}^2 - \mathrm{D}^2)\tilde{u} + \mathrm{D}\tilde{P} + \tilde{e}_{10}\widetilde{Ra}_m\widetilde{Pr}\mathrm{D}\tilde{H}_{x0}\tilde{\theta} + \widetilde{Ra}_m\widetilde{Pr}\tilde{\theta}_0\tilde{e}_{10}\mathrm{D}^2\tilde{\phi} \\ & + \widetilde{Ra}_m\widetilde{Pr}\tilde{\theta}_0\left[\mathrm{i}\tilde{\alpha}\tilde{e}_{20} + (1-\tilde{e}_{10}^2)\frac{\mathrm{D}\tilde{H}_{x0}}{\tilde{H}_0}\right]\mathrm{D}\tilde{\phi} - \mathrm{i}\tilde{\alpha}\widetilde{Ra}_m\widetilde{Pr}\tilde{\theta}_0\tilde{e}_{10}\tilde{e}_{20}\frac{\mathrm{D}\tilde{H}_{x0}}{\tilde{H}_0}\tilde{\phi} = 0, \end{aligned} \tag{6.3}$$

$$\tilde{\sigma}\tilde{v} + \widetilde{Pr}(\tilde{\alpha}^2 - \mathrm{D}^2)\tilde{v} + \mathrm{i}\tilde{\alpha}\tilde{P} + \tilde{\alpha}\widetilde{Ra}_m\widetilde{Pr}\tilde{\theta}_0(\mathrm{i}\tilde{e}_{10}\mathrm{D}\tilde{\phi} - \tilde{\alpha}\tilde{e}_{20}\tilde{\phi}) = 0, \tag{6.4}$$

$$\widetilde{\sigma}\widetilde{w}+\widetilde{Pr}(\widetilde{\alpha}^2-\mathrm{D}^2)\widetilde{w}+\mathrm{i}\widetilde{\beta}\widetilde{P}+\widetilde{\beta}\widetilde{Ra}_m\widetilde{Pr}\widetilde{\theta}_0(\mathrm{i}\widetilde{e}_{10}\mathrm{D}\widetilde{\phi}-\widetilde{\alpha}\widetilde{e}_{20}\widetilde{\phi})=0, \tag{6.5}$$

$$\widetilde{\sigma}\widetilde{\theta}+\mathrm{D}\widetilde{\theta}_0\widetilde{u}+(\widetilde{\alpha}^2-\mathrm{D}^2)\widetilde{\theta}=0, \tag{6.6}$$

$$\begin{aligned}0=&(\mathrm{D}^2-\widetilde{\alpha}^2)\widetilde{\phi}+(1-\widetilde{e}_{10}^2)\left(\frac{\widetilde{\chi}_*-\widetilde{\chi}}{1+\widetilde{\chi}}\widetilde{N}-\widetilde{\theta}_0\right)\frac{\mathrm{D}^2\widetilde{\phi}}{\widetilde{H}_0}\\&-\left[(1-\widetilde{e}_{10}^2)\mathrm{D}\widetilde{\theta}_0+\widetilde{e}_{10}\left(\frac{\widetilde{\chi}_*-\widetilde{\chi}}{1+\widetilde{\chi}}\widetilde{N}-\widetilde{\theta}_0\right)\left(2\mathrm{i}\widetilde{\alpha}\widetilde{e}_{20}+3(1-\widetilde{e}_{10}^2)\frac{\mathrm{D}\widetilde{H}_{x0}}{\widetilde{H}_0}\right)\right]\frac{\mathrm{D}\widetilde{\phi}}{\widetilde{H}_0}\\&-\left[\left(\frac{\widetilde{\chi}_*-\widetilde{\chi}}{1+\widetilde{\chi}}\widetilde{N}-\widetilde{\theta}_0\right)\left(\widetilde{\alpha}^2(1-\widetilde{e}_{20}^2)+\mathrm{i}\widetilde{\alpha}\widetilde{e}_{20}(1-3\widetilde{e}_{10}^2)\frac{\mathrm{D}\widetilde{H}_{x0}}{\widetilde{H}_0}\right)\right.\\&\left.-\mathrm{i}\widetilde{\alpha}\widetilde{e}_{20}\widetilde{e}_{10}\mathrm{D}\widetilde{\theta}_0\right]\frac{\widetilde{\phi}}{\widetilde{H}_0}-\left(\mathrm{i}\widetilde{\alpha}\widetilde{e}_{20}+(1-\widetilde{e}_{10}^2)\frac{\mathrm{D}\widetilde{H}_{x0}}{\widetilde{H}_0}\right)\widetilde{\theta}-\widetilde{e}_{10}\mathrm{D}\widetilde{\theta},\end{aligned} \tag{6.7}$$

with the boundary conditions

$$\begin{aligned}&\left(1+\widetilde{\chi}+(1-\widetilde{e}_{10}^2)\frac{(\widetilde{\chi}_*-\widetilde{\chi})\widetilde{N}\pm(1+\widetilde{\chi})}{\widetilde{H}_0}\right)\mathrm{D}\widetilde{\phi}\\&\pm|\widetilde{\alpha}|\widetilde{\phi}-\mathrm{i}\widetilde{\alpha}\widetilde{e}_{10}\widetilde{e}_{20}\frac{(\widetilde{\chi}_*-\widetilde{\chi})\widetilde{N}\pm(1+\widetilde{\chi})}{\widetilde{H}_0}\widetilde{\phi}=0,\end{aligned} \tag{6.8}$$

$$\widetilde{u}=\widetilde{v}=\widetilde{w}=\widetilde{\theta}=0\quad\text{at }\bar{x}=\pm1. \tag{6.9}$$

Equation (6.4) is obtained by multiplying (5.5) by α, (5.6) by β, adding them together, and dividing the result by $\widetilde{\alpha}$. Note that only (6.5) contains $\widetilde{w}$ and $\widetilde{\beta}$ and thus it can be solved for any particular value of $\widetilde{\beta}$ after $\widetilde{\sigma}$, $\widetilde{P}$ and $\widetilde{\phi}$ are found from (6.2)–(6.4), (6.6) and (6.7), which form an equivalent two-dimensional problem obtained by formally setting $\widetilde{w}=\widetilde{\beta}=0$. It is important to note though that the notion of an equivalent two-dimensional problem in the current context is somewhat different from that arising in problems dealing with non-magnetic fluids. The reason is that even if $\widetilde{w}$ and $\widetilde{\beta}$ are set to zero in the above Squire-transformed equations the external magnetic field remains three-dimensional. In general it still has three non-zero components in the x, y and z directions and thus it needs to be described using two coordinate angles δ and γ that act as independent control parameters of the problem. The above transformations simply mean that we conveniently view the y direction as the periodicity direction of the perturbation structures that arise, while the vector of the applied magnetic field can be arbitrarily oriented. More specifically, the axes of the instability rolls are considered to be always parallel to the z axis in figure 1 so that $\gamma=0^\circ$ ($\gamma=90^\circ$) means that the magnetic field has a component in the plane of the fluid layer that is perpendicular (parallel) to the roll axes. The values of $0^\circ<\gamma<90^\circ$ are interpreted accordingly. For the sake of brevity in the following sections we will for convenience refer to instability patterns computed using the above transformed equations for $\gamma=0^\circ$ and $\gamma=90^\circ$ as transverse and longitudinal rolls, respectively, while patterns obtained for all other values of γ will be referred to as oblique rolls. We will also refer to angle δ as the field inclination angle and angle γ as the angle between the axes of the instability rolls and the in-layer component of the applied magnetic field.

7. Numerical results

7.1. *Discretisation*

Equations (6.2)–(6.7) are discretised using the pseudo-spectral Chebyshev collocation method as introduced in Ku & Hatziavramidis (1984), Hatziavramidis & Ku (1985) and implemented in Suslov & Paolucci (1995*a*,*b*). This spatial approximation converges exponentially quickly so that 71 collocation points used in the current computations guarantee that all digits in the reported numerical results are significant and accurate. Upon discretisation and exclusion of (6.5), which is the only equation containing β, the system of (6.2)–(6.7) results in a generalised algebraic eigenvalue problem for the complex amplification rate $\widetilde{\sigma}$

$$(\widetilde{\sigma}\boldsymbol{X} + \boldsymbol{Y})\boldsymbol{q} = \boldsymbol{0}, \tag{7.1}$$

where $\boldsymbol{X}$ and $\boldsymbol{Y} = Y(\widetilde{\sigma}, \widetilde{Ra_m}, \widetilde{Pr}, \widetilde{\chi}, \widetilde{\chi}_*; \delta, \gamma)$ are matrices and eigenvector $\boldsymbol{q}$ contains the discretised components of $(\widetilde{u}, \widetilde{v}, \widetilde{P}, \widetilde{\theta}, \widetilde{\phi})^{\mathrm{T}}$. The eigenvalue problem is solved using the MATLAB (MATLAB 2013) function `eig`. Once both $\widetilde{\sigma}$ and $\boldsymbol{q}$ are found (6.5) is written as

$$\left(Pr\left(\mathrm{D}^2 - \widetilde{\alpha}^2\right) - \widetilde{\sigma}\right)\widetilde{w} = \mathrm{i}\widetilde{\beta}\left(\widetilde{P} + \widetilde{Ra_m}\widetilde{Pr}\widetilde{\theta}_0\left(\widetilde{e}_{10}\mathrm{D}\widetilde{\phi} + \mathrm{i}\widetilde{\alpha}\widetilde{e}_{20}\widetilde{\phi}\right)\right) \tag{7.2}$$

and solved for $\widetilde{w}$. The inverse Squire's transformation (6.1) then recovers full three-dimensional solutions for perturbations.

7.2. *Check of numerical accuracy*

In order to test the numerical code, the critical values for the magnetic convection threshold in a perpendicular ($\delta = 0°$) external magnetic field with magnitude $H^e = 100$ for the case of $\widetilde{Pr} = 130$ and $\widetilde{\chi} = \widetilde{\chi}_* = 4$ have been computed using relation (3.11), and the critical values $\widetilde{Gr}_{mc} = 1.387$ and $\widetilde{\alpha}_c = 1.928$ are obtained, which agree well with the values of $\widetilde{Gr}_{mc} = 1.385$ and $\widetilde{\alpha}_c = 1.95$ computed from the corresponding data reported in Finlayson (1970). The magnetic convection threshold for $\widetilde{Pr} = 130$ and $\widetilde{\chi} = \widetilde{\chi}_* = 5$ is also determined and the critical values $\widetilde{Gr}_{mc} = 1.3981$ and $\widetilde{\alpha}_c = 1.9365$ are obtained, which are identical to those reported in Suslov (2008). As an additional check the critical values of $\widetilde{Ra}_{mc} = 160.543$ and $\widetilde{\alpha}_c = 1.8045$ were computed for the normal field $H^e = 100$ in the limit of a paramagnetic fluid with $\widetilde{\chi} = \widetilde{\chi}_* = 10^{-3}$. These values are in excellent agreement with the respective values of $2568.476/16 = 160.530$ and $3.609/2 = 1.8045$ reported in Huang *et al.* (1997) (the coefficients of $1/16$ and $1/2$ are due to the differences between the non-dimensionalisation scales used).

7.3. *Flow stability characteristics*

The numerical values of critical parameters for thermomagnetic convection arising in magnetic fields of various orientations and intensities are given in tables 2–4. The data in the tables warrant a number of general conclusions.

The magneto-convective instability arising in a normal field remains stationary regardless of the specific magnetic properties of the fluid and the magnitude of the applied magnetic field. This is in agreement with the findings previously reported, for example, in Finlayson (1970), Huang *et al.* (1997) and Suslov (2008). However, in contrast to all previous studies, the instability threshold $\widetilde{Ra}_{mc}$ is found to depend

$\widetilde{\chi}$	$\widetilde{\chi}_*$	$\widetilde{\alpha}_c$	$\widetilde{Ra}_{mc}$	$\widetilde{c}_c$	Σ_k	Re(Σ_{m1})	Im(Σ_{m1})
5	5	1.936	181.7	0	0.0982	1.584	0
		1.920	178.0	0	0.0984	1.559	0
3	5	1.860	159.3	0	0.0997	1.424	0
		1.846	157.0	0	0.0998	1.407	0
3	3	1.915	178.3	0	0.0985	1.565	0
		1.909	176.8	0	0.0986	1.554	0
1.5	2.5	1.847	159.1	0	0.0998	1.427	0
		1.843	158.3	0	0.0998	1.421	0
1	3	1.797	145.9	0	0.1007	1.325	0
		1.792	145.1	0	0.1007	1.320	0
1	2	1.827	155.0	0	0.1001	1.397	0
		1.825	154.5	0	0.1001	1.393	0
0.5	1.5	1.801	150.0	0	0.1005	1.357	0
		1.799	149.2	0	0.1005	1.355	0

TABLE 2. The critical values of $\widetilde{Ra}_m$, $\widetilde{\alpha}$ and disturbance wave speed $\widetilde{c} = -\widetilde{\sigma}^I/\widetilde{\alpha}$ and the corresponding perturbation energy integrals Σ_k and Σ_{m1} for magnetoconvection at $\delta = 0°$, $H^e = 100$ (odd-numbered lines), $H^e = 10$ (even-numbered lines) and various values of $\widetilde{\chi}$ and $\widetilde{\chi}_*$.

$\widetilde{\chi}$	$\widetilde{\chi}_*$	$\widetilde{\alpha}_c$	$\widetilde{Ra}_{mc}$	$\widetilde{c}_c$	Σ_k	Re(Σ_{m1})	Im(Σ_{m1})
5	5	2.428	2049	0.0256	0.0506	1.9562	−0.0037
		2.468	1935	0.2048	0.0505	1.9993	−0.0354
3	5	2.510	2796	0.0279	0.0472	1.7755	−0.0026
		2.534	2577	0.2332	0.0476	1.8146	−0.0273
3	3	2.116	533.8	−0.0011	0.0822	2.2432	−0.0044
		2.135	548.3	−0.0085	0.0809	2.2420	−0.0421
1.5	2.5	2.051	433.2	−0.0012	0.0873	2.0035	−0.0029
		2.061	439.8	−0.0108	0.0866	2.0058	−0.0287
1	3	2.221	724.9	0.0018	0.0757	1.9704	−0.0033
		2.228	721.9	0.0167	0.0750	1.9575	−0.0321
1	2	1.967	329.4	−0.0014	0.0926	1.8328	−0.0019
		1.973	333.5	−0.0139	0.0923	1.8391	−0.0192
0.5	1.5	1.894	259.3	−0.0012	0.0962	1.6545	−0.0012
		1.898	261.4	−0.0121	0.0960	1.6594	−0.0115

TABLE 3. Same as table 2 but for transverse rolls at $\delta = 10°$ and $\gamma = 0°$.

not only on the values of the magnetic susceptibilities χ and χ_* but also on the magnitude of the applied magnetic field, namely, the decrease of the characteristic non-dimensional field parameter N promotes instability and increases the wavelength of the patterns that arise. This dependence, however, remains relatively weak: the largest difference between the critical values of magnetic Rayleigh numbers and wavenumbers is found to be under 3.5 % and 1.5 %, respectively, for a fluid with the highest degree of magnetisation investigated ($\chi = \chi_* = 5$) when the external magnetic field is changed by a factor of 10. The comparison of the current results with our previous study (Suslov 2008) shows that the dependence of the critical parameters on the magnitude of the magnetic field is traced back to the form of the constitutive magnetisation (2.7). Its linearisation used in all previous studies cited

$\widetilde{\chi}$	$\widetilde{\chi}_*$	$\widetilde{\alpha}_c$	$\widetilde{Ra}_{mc}$	$\widetilde{c}_c$	Σ_k	Re(Σ_{m1})	Im(Σ_{m1})
5	5	1.937	385.2	0	0.0982	1.5844	0
		1.943	389.6	0	0.0978	1.6117	0
3	5	1.903	458.9	0	0.0988	1.5105	0
		1.908	457.2	0	0.0984	1.5258	0
3	3	1.916	267.0	0	0.0985	1.5650	0
		1.917	270.3	0	0.0985	1.5747	0
1.5	2.5	1.865	251.6	0	0.0995	1.4640	0
		1.866	253.5	0	0.0994	1.4693	0
1	3	1.842	313.1	0	0.0999	1.4094	0
		1.844	313.7	0	0.0997	1.4146	0
1	2	1.844	226.5	0	0.0998	1.4315	0
		1.845	227.8	0	0.0998	1.4346	0
0.5	1.5	1.816	203.2	0	0.1002	1.3879	0
		1.817	204.1	0	0.1003	1.3893	0

TABLE 4. Same as table 2 but for longitudinal rolls at $\delta = 10°$ and $\gamma = 90°$.

above eliminates the dependence of the threshold values on the amplitude of the normal magnetic field. However, as shown in § 4 such an idealisation is only robust for the case of paramagnetic fluids with small magnetic susceptibilities but it should not be expected to be uniformly valid for realistic ferromagnetic fluids.

If the dependence of the fluid magnetisation on the magnitude of the applied magnetic field remains linear, that is if $\chi \approx \chi_*$, see figure 2, then the magnetoconvection threshold parameters decrease monotonically with the values of magnetic susceptibilities to their limiting values $(\widetilde{Ra}_{mc}, \widetilde{\alpha}_c) \approx (160.5, 1.805)$ that are independent of the magnitude of the applied magnetic field. However, when the fluid magnetisation approaches saturation so that $\chi < \chi_*$, the variation of the differential and integral susceptibilities have opposite influences on the threshold: the decrease of χ at fixed χ_* promotes instability while the decrease of χ_* at fixed χ delays it. In realistic ferrofluids, however, the values of both χ and χ_* decrease with the increasing magnetic field, but at different rates, see figure 2(*a*). Therefore, it is not straightforward to anticipate what the overall effect of a changing magnetic field on the convection onset could be and one needs to rely on the specific computational results. In particular, the data in table 2 show that the critical value of magnetic Rayleigh number decreases by more than 10 % when progressively stronger magnetic field is applied to a layer of experimental ferrofluid with the initial susceptibilities $\chi = \chi_* \approx 3$ that are reduced to $\chi \approx 1.5$ and $\chi_* \approx 2.5$ during a typical experimental run.

It is remarkable that, as seen from tables 3 and 4, when an oblique magnetic field is applied to the layer the trends described above are reversed even for small field inclination angles δ: now the decrease of χ at fixed χ_* delays instability while the decrease of χ_* at fixed χ promotes it. This indicates the qualitative difference between the instability mechanisms present in normal and oblique fields that we will discuss in more detail in the following sections. The numerical data given in tables 2–4 also demonstrate a very strong stabilisation effect of the field inclination compared to the normal field situation that is further illustrated in figures 6(*a*) and 8(*a*). Such a stabilisation is observed regardless of the specific magnetic properties of the fluid for all investigated values of χ and χ_*.

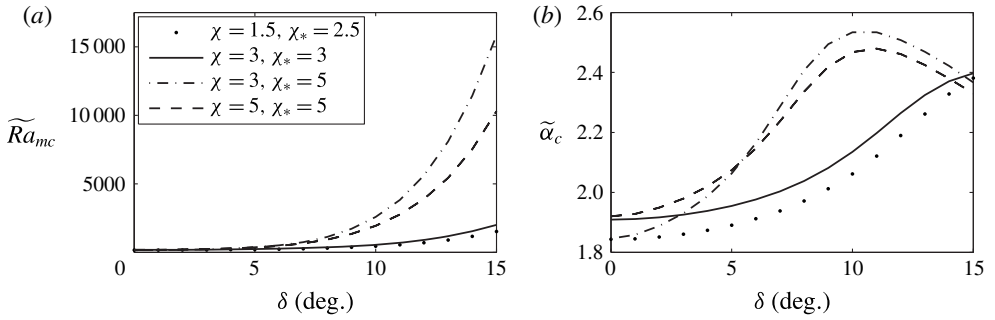

FIGURE 6. (*a*) Critical magnetic Rayleigh number $\widetilde{Ra}_{mc}$ and (*b*) wavenumber $\widetilde{\alpha}_c$ as functions of the field inclination angle δ for transverse rolls at $H^e = 10$ and $\gamma = 0°$. The respective plots for $H^e = 100$ are indistinguishable within the figure resolution.

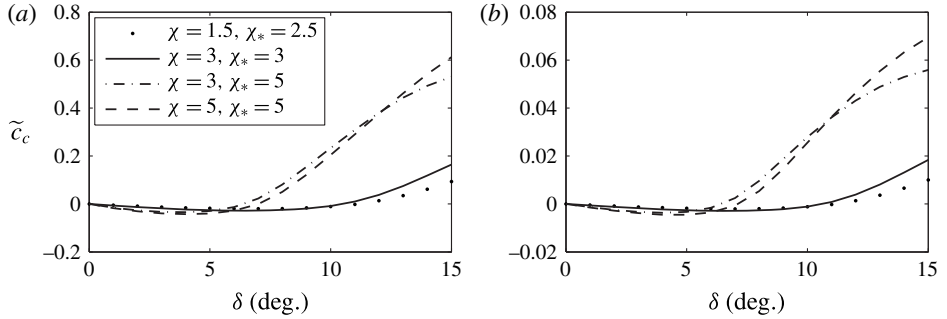

FIGURE 7. Critical wave speed $\widetilde{c} = -\widetilde{\sigma}^I/\widetilde{\alpha}_c$ as a function of the field inclination angle δ for transverse rolls at $\gamma = 0°$ for (*a*) $H^e = 10$ and (*b*) $H^e = 100$.

An even more striking effect of the field inclination is evident from the data presented in table 3: the transverse instability rolls computed for $\gamma = 0°$ become oscillatory resulting in waves propagating along the direction of the field component that is tangential to the plane of the fluid layer. This is a somewhat unexpected result given that the unperturbed problem possesses a full planar symmetry with no preferred direction. Moreover Huang *et al.* (1997) even argued that the instability in this problem can only be stationary. The resolution of this apparent paradox is prompted by the comparative computational data presented in table 3 for $H^e = 10$ and $H^e = 100$ and by figure 7. They show that the magnitude of the disturbance wave speed $|\widetilde{c}| = |\sigma^I/\widetilde{\alpha}_c|$ is approximately inversely proportional to the magnitude of the applied magnetic field H^e, which in turn is proportional to the field parameter N characterising the nonlinearity of the magnetic field distribution within a layer. It is assumed in Huang *et al.* (1997) that $N \to \infty$ and effectively postulated that the magnetic field within the layer varies linearly. No unsteady patterns were found there. Therefore, we conclude that the main reason for the appearance of oscillatory instability in the current problem is the nonlinearity of the magnetic field within the ferrofluid layer as has been discussed in § 4.

The values of the threshold parameters for longitudinal rolls computed for $\gamma = 90°$ are given in table 4. Remarkably, they remain strictly stationary for all values of the governing parameters. Figure 8(*a*) shows that, similar to the critical magnetic Rayleigh

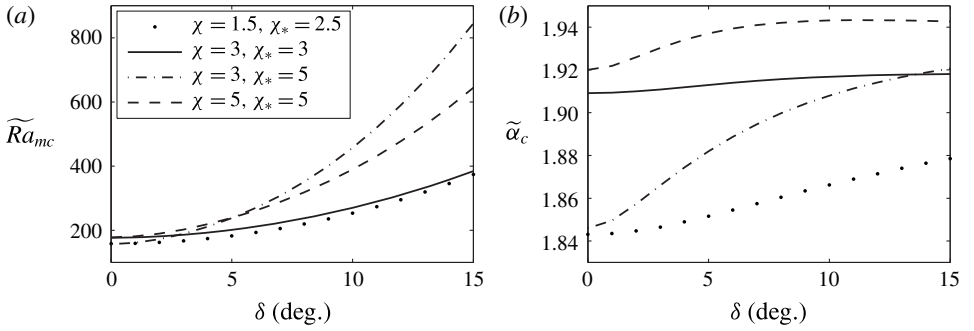

FIGURE 8. Same as figure 6 but for longitudinal rolls at $\gamma = 90°$.

number for transverse rolls, the one for longitudinal rolls increases quickly with the field inclination angle δ. However, for all non-zero angles it remains smaller than that of transverse rolls. This is consistent with findings of Huang *et al.* (1997) for paramagnetic fluids and confirms an experimental fact that the axes of thermomagnetic rolls appearing away from the boundaries always align with the tangential component of the magnetic field since this configuration is found to be less stable than a transverse one. Having said this, we emphasise that even though longitudinal rolls are always expected to dominate the observed instability patterns, the possibility of the existence of transverse rolls should not be ignored for at least two reasons. Firstly, unlike in paramagnetic fluids, in ferrofluids they are qualitatively different from their longitudinal counterparts as they are unsteady. They are also characterised by a wavenumber that depends sensitively on the field inclination angle, see figure 6(*b*), while the wavenumber of longitudinal rolls remains almost constant as the field inclination is increased, see figure 8(*b*). Secondly, near the boundaries of a layer the longitudinal rolls may be suppressed due to the geometry of the boundary or other influences that are not present in unbounded domains so that oscillatory transverse rolls might be preferred. The experimental observations reported in our previous work (Suslov *et al.* 2012) (see figures 9 and 11 there) indeed indicate that this might have been the case in the near-boundary regions of a finite experimental enclosure.

Given that the two limiting cases of transverse and longitudinal rolls have qualitatively different characteristics it is of interest to investigate how and at what value of the intermediate angle the transition between stationary and oscillatory patterns occurs. Thus we have computed the stability characteristics of oblique rolls for various values of magnetic susceptibilities and field inclination angles. These are presented in figures 9–11. They confirm that both the critical magnetic Rayleigh number and wavenumber increase continuously and monotonically from longitudinal to transverse rolls and the rate at which they do grows quickly with the field inclination angle. The only exception is the behaviour of the wavenumber for relatively large field inclination angles when it reaches its maximum value for oblique rolls forming an angle of about 45° with the tangential field component and then starts decreasing. Of particular interest is the behaviour of the disturbance wave speed. It grows continuously from zero for longitudinal rolls to its maximum for transverse rolls; however, the most rapid growth is observed for $\gamma \lesssim 50°$ and $\gamma \gtrsim 130°$. This suggests that if the value of magnetic Rayleigh number is gradually increased in an experiment then the stationary rolls aligned with the tangential component of the field will appear first. Subsequently, they would be unsteadily modulated by a periodic

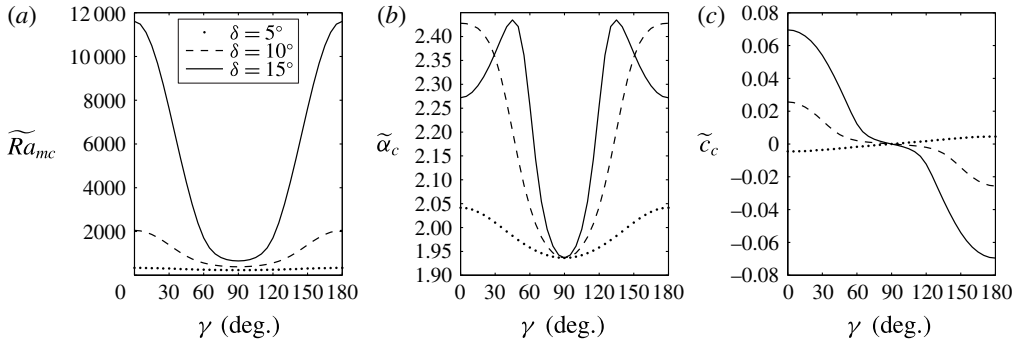

FIGURE 9. (*a*) Critical magnetic Rayleigh number $\widetilde{Ra}_{mc}$, (*b*) wavenumber $\widetilde{\alpha}_c$ and (*c*) wave speed $\tilde{c}$ as functions of the azimuthal angle γ for various angles δ for $H^e = 100$ and $\widetilde{\chi} = \widetilde{\chi}_* = 5$.

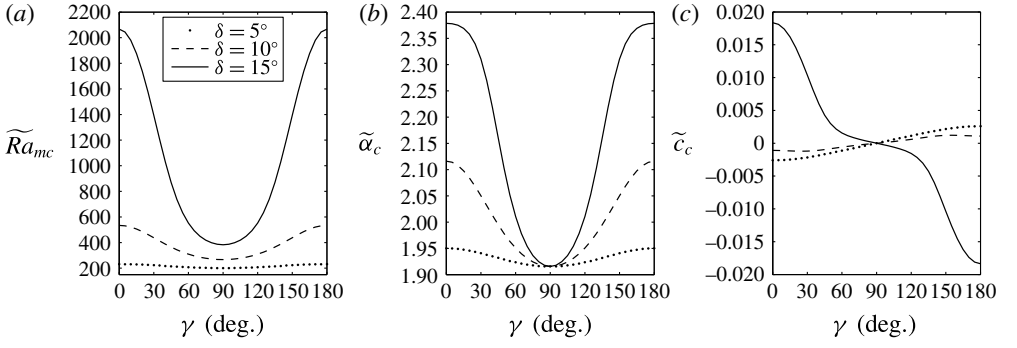

FIGURE 10. Same as figure 9 but for $\widetilde{\chi} = \widetilde{\chi}_* = 3$.

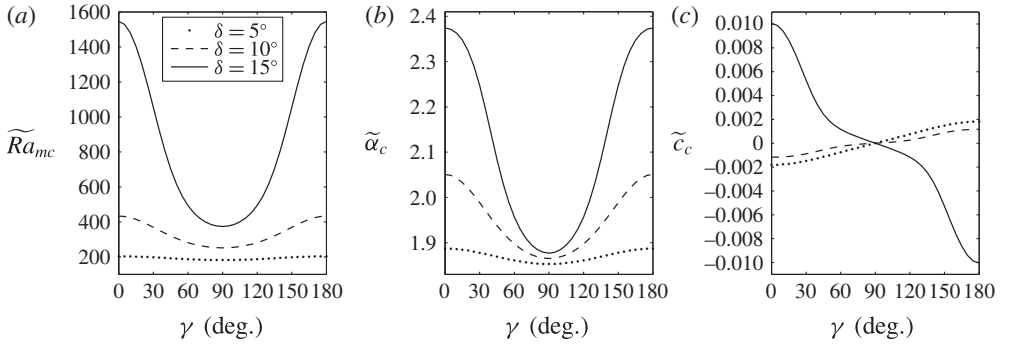

FIGURE 11. Same as figure 9 but for $\widetilde{\chi} = 1.5$ and $\widetilde{\chi}_* = 2.5$.

pattern forming an angle of about 40–45° with the axes of the stationary rolls. A further increase of magnetic Rayleigh number would lead to the increase of the modulation frequency and wavenumber and to the re-orientation of the modulating pattern so that it would become closer to orthogonal with respect to the original stationary rolls.

It is also noteworthy that the $\widetilde{Ra}_{mc}$ and $\widetilde{\alpha}_c$ curves are symmetric with respect to the $\gamma = 90°$ line, while the $\widetilde{c}_c$ line is centro-symmetric with respect to $(\widetilde{c}_c,\ \gamma) = (0, 90°)$. To shed light on why this is so refer to figure 5(*a*,*c*) where the concave south–west/north–east magnetic field lines are shown for $\gamma = 0°$. If γ is changed to 180° the magnetic field lines re-orient to become north–west/south–east and convex. As has been discussed above, the appearance of oscillatory disturbances is a consequence of the nonlinearity of the magnetic field. Therefore we conclude that it is this change of the curvature of magnetic lines in the plane perpendicular to the roll axes that is responsible for the change of the sign of the disturbance wave speed.

7.4. *Perturbation energy balance*

To confirm the physical nature of the observed instabilities it is instructive to consider the mechanical energy balance in a way similar to that used for example in Hart (1971), Suslov & Paolucci (1995*a*), Suslov, Bozhko & Putin (2008) and Suslov *et al.* (2012). We multiply the momentum equations (6.3) and (6.4) by the complex-conjugate velocity components $\bar{u}$ and $\bar{v}$, respectively, add them together and integrate by parts across the layer using the boundary conditions (6.9) and the continuity equation (6.2) to obtain

$$\widetilde{\sigma}\,\Sigma_k = \Sigma_{vis} + \Sigma_{m1} + \Sigma_{m2}, \tag{7.3}$$

where

$$\Sigma_k = \int_{-1}^{1} \underbrace{(|\widetilde{u}|^2 + |\widetilde{v}|^2)}_{E_k}\,\mathrm{d}\bar{x} > 0, \tag{7.4a}$$

$$\Sigma_{vis} = \int_{-1}^{1} \underbrace{-\widetilde{Pr}(\widetilde{\alpha}^2(|\widetilde{u}|^2 + |\widetilde{v}|^2) + |\mathrm{D}\widetilde{u}|^2 + |\mathrm{D}\widetilde{v}|^2)}_{E_{vis}}\,\mathrm{d}\bar{x} = -1, \tag{7.4b}$$

$$\Sigma_{m1} = \int_{-1}^{1} \underbrace{-\widetilde{Ra}_m\widetilde{Pr}\mathrm{D}\widetilde{H}_{x0}\widetilde{e}_{10}\widetilde{\theta}\bar{\widetilde{u}}}_{E_{m1}}\,\mathrm{d}\bar{x}, \tag{7.4c}$$

$$\Sigma_{m2} = \int_{-1}^{1} E_{m2}\mathrm{d}\bar{x} \tag{7.4d}$$

and

$$\begin{aligned} E_{m2} = {} & -\widetilde{Ra}_m\widetilde{Pr}\mathrm{D}\widetilde{H}_{x0}\bar{\widetilde{u}}\frac{\widetilde{\theta}_0}{\widetilde{H}_0}\left((1-\widetilde{e}_{10}^2)\mathrm{D}\widetilde{\phi} - \mathrm{i}\widetilde{\alpha}\widetilde{e}_{10}\widetilde{e}_{20}\widetilde{\phi}\right) \\ & - \widetilde{Ra}_m\widetilde{Pr}\widetilde{\theta}_0\left(\widetilde{e}_{10}\bar{\widetilde{u}}\mathrm{D}^2\widetilde{\phi} + \mathrm{i}\widetilde{\alpha}(\widetilde{e}_{10}\bar{\widetilde{v}} + \widetilde{e}_{20}\bar{\widetilde{u}})\mathrm{D}\widetilde{\phi} - \widetilde{\alpha}^2\widetilde{e}_{20}\bar{\widetilde{v}}\widetilde{\phi}\right). \end{aligned} \tag{7.5}$$

Given that Σ_k is positive definite, the perturbation energy balance (7.3) determines the complex growth rate σ of linear instability. It does not contain the modified pressure P as it integrates to zero identically. This confirms that the potential component of the Kelvin force included in P indeed has no effect on the stability of a layer of ferromagnetic fluid as has been stated in § 2. The viscous dissipation contribution to the energy perturbation balance is always negative and, given that the eigenfunctions of the linearised problem are defined up to a multiplicative constant, we scale

them in such a way that $\Sigma_{vis} \equiv -1$. The remaining two terms are of magnetic nature. As discussed in Suslov *et al.* (2012), Σ_{m1} represents the variation of fluid magnetisation (and thus of the local Kelvin force) due to the thermal perturbations while Σ_{m2} describes the energy contribution associated with the induced magnetic field variations. Separating the real (Re) and imaginary (Im) parts of (7.3) we obtain at the critical point

$$0 = \mathrm{Re}(\Sigma_{m1} + \Sigma_{m2}) - 1, \quad \widetilde{\sigma}^I \Sigma_k = \mathrm{Im}(\Sigma_{m1} + \Sigma_{m2}). \tag{7.6a,b}$$

The energy terms with positive real parts promote instability, while the ones with negative suppress it. Equation (7.6*b*) demonstrates that the nature of the detected oscillatory instabilities is purely magnetic.

Tables 2–4 contain numerical data for various perturbation energy terms that enable us to draw a number of general conclusions. Firstly, the magnitude of the kinetic energy term Σ_k never exceeds the value of about 10 % of the viscous dissipation, while the magnitude of the magnetic contribution Σ_{m1} always exceeds the dissipation value. This confirms that the instability is of magnetic rather than hydrodynamic or thermal nature and that the visible fluid motion triggered by the instability is not the main recipient of the energy supplied to the system (in experiments such as those described in Suslov *et al.* (2012) the energy is supplied by heat exchangers attached to the layer walls). Secondly, since $\mathrm{Re}(\Sigma_{m1})$ is always positive we conclude that the specific mechanism triggering the instability is the thermally induced variation of fluid magnetisation. Thirdly, since $\mathrm{Re}(\Sigma_{m1}) > 1$ then, according to (7.6*a*), $\mathrm{Re}(\Sigma_{m2}) < 0$. This means that the variation of the applied magnetic field caused by perturbations always plays a stabilising role. In summary, the analysis of mechanical energy balance shows that the energy received by the system through a thermal exchange with the ambient is mostly spent on varying the local magnetisation of the fluid. In turn the latter triggers fluid motion, which is an observable signature of instability. The remaining part of the received energy is spent on modifying the magnetic field. Since the variation of magnetic field is not limited to the interior of the layer this energy largely leaves it and thus cannot be used for supporting a mechanical instability within the system.

Typical distributions of the perturbation energy integrands for instability patterns arising in normal and oblique fields are shown in figures 12 and 13, respectively. Since the integrand behaviour for longitudinal rolls is found to be qualitatively similar to that for stationary rolls arising in a normal field, only the results for transverse rolls are presented here. As expected, the viscous dissipation E_{vis} occurs mostly near the solid boundaries and the kinetic energy E_k of perturbations is maximised near the centre of the layer. Figures 12(*b*) and 13(*b*) show that the magnetisation variation effect E_{m1} plays a destabilising role uniformly across the complete width of the layer and with the maximum near its centre. On the other hand, the stabilising effect of magnetic field modification E_{m2} is most pronounced near the walls of the layer. This is intuitively expected since the internal magnetic field near the walls defines the external field via the field-matching boundary conditions (5.12) and (5.13). The overall role of the E_{m1} and E_{m2} effects does not change in the oblique field; however, the field inclination introduces a noticeable asymmetry. The maximum of the destabilising influence shifts toward the hot wall: compare the locations of the maxima of the dash-dotted lines in figures 12(*b*) and 13(*b*). This is because the unstable magnetic buoyancy stratification in oblique fields is more pronounced near the hot wall, see figure 5(*b,d*) and the discussion in § 4. While the magnitude of $\mathrm{Re}(E_{m1})$ determines whether the instability is present, figure 13(*c*) shows that it is the magnitude of $\mathrm{Im}(E_{m2})$ that predominantly defines the sign of $\widetilde{\sigma}^I$ and thus the propagation direction of transverse and oblique rolls.

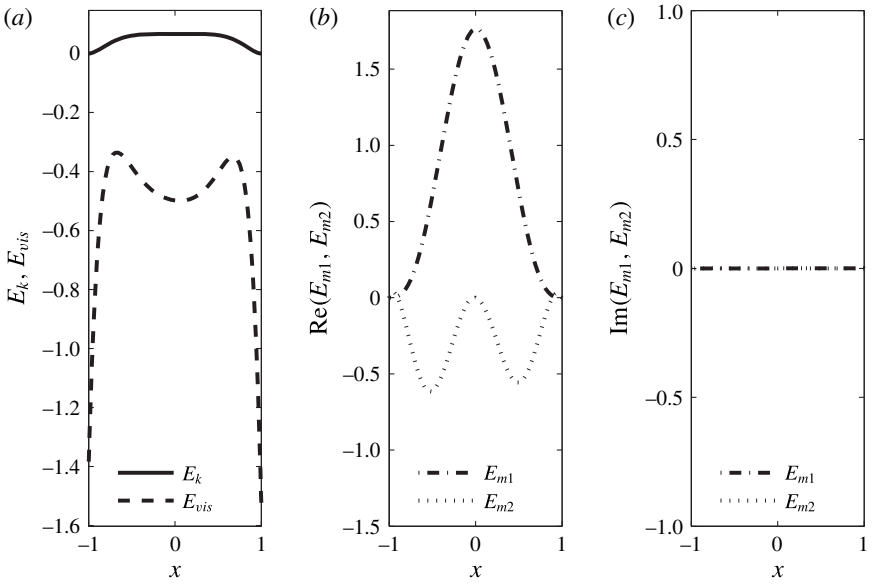

FIGURE 12. Disturbance energy integrands at the critical point of magnetoconvection threshold $\widetilde{Ra}_{mc} = 176.8$, $\widetilde{\alpha}_c = 1.909$ at $H^e = 10$, $\delta = \gamma = 0°$ and $\chi = \chi_* = 3$.

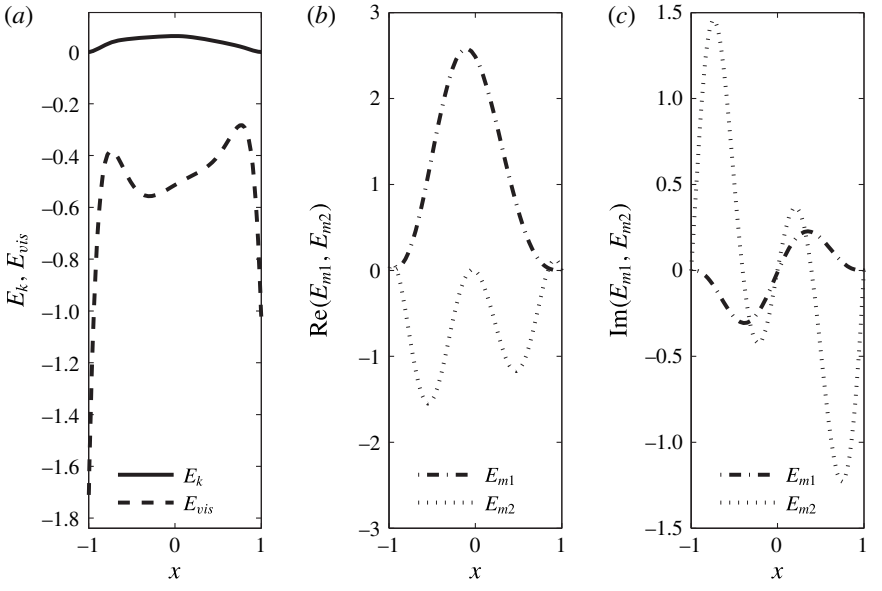

FIGURE 13. Same as figure 12 but for $\widetilde{Ra}_{mc} = 548.4$, $\widetilde{\alpha}_c = 2.135$, $\delta = 10°$.

7.5. *Perturbation fields*

To complete this report we present the plots of typical perturbation fields arising in normal and inclined magnetic fields. The mechanism driving convection is straightforward to see from figure 14 for a normal field. Consider, for example, the region near $y = 3$. There the thermal perturbation θ_1 leads to local cooling. As a

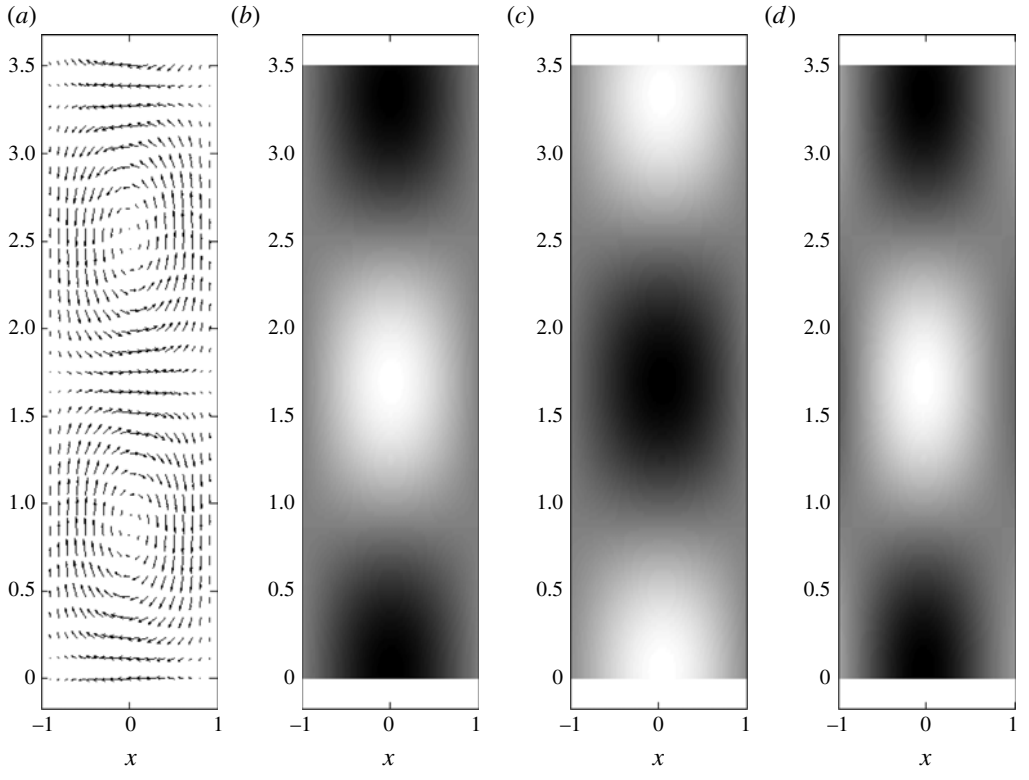

FIGURE 14. Perturbation eigenfunctions of (*a*) the fluid velocity $\boldsymbol{v}_1 = (u, v)$, (*b*) temperature θ_1, (*c*) magnetisation M_1 and (*d*) magnetic field H_1, for magnetoconvection at $H^e = 10$, $\delta = \gamma = 0°$ and $\widetilde{\chi} = \widetilde{\chi}_* = 3$ at the critical point $\widetilde{Ra}_{mc} = 176.8$, $\widetilde{\alpha}_c = 1.909$. The field values increase from black to white.

result this region becomes more strongly magnetised, see figure 14(*c*) for M_1, and the fluid there is driven toward the hot wall where the basic magnetic field is stronger, see figure 3(*a,d*). This is reflected in the plot of the velocity field (figure 14*a*) showing that indeed cool fluid flows toward the hot wall (from right to left) there. This situation is similar to gravitational convection arising in a fluid heated from below.

When the applied magnetic field is inclined the mechanism driving convection remains the same, even though it is less straightforward to recognise it from figure 15. The thermal and magnetisation perturbation cells align with the applied magnetic field and so does the main fluid flow direction.

It is noteworthy that the perturbation cells for magnetic field H_1 corresponding to transverse rolls do not align with the rest of the perturbation field, see figure 15(*d*). They also become asymmetric. At the same time the structure of the perturbation fields for longitudinal rolls in an inclined field (not shown) remains very similar to that seen in figure 14 for a normal field. Therefore, it is logical to conclude that the phase shift between the magnetic field H_1 and the rest of the perturbation fields is responsible for the change of the instability character to oscillatory for transverse and oblique rolls.

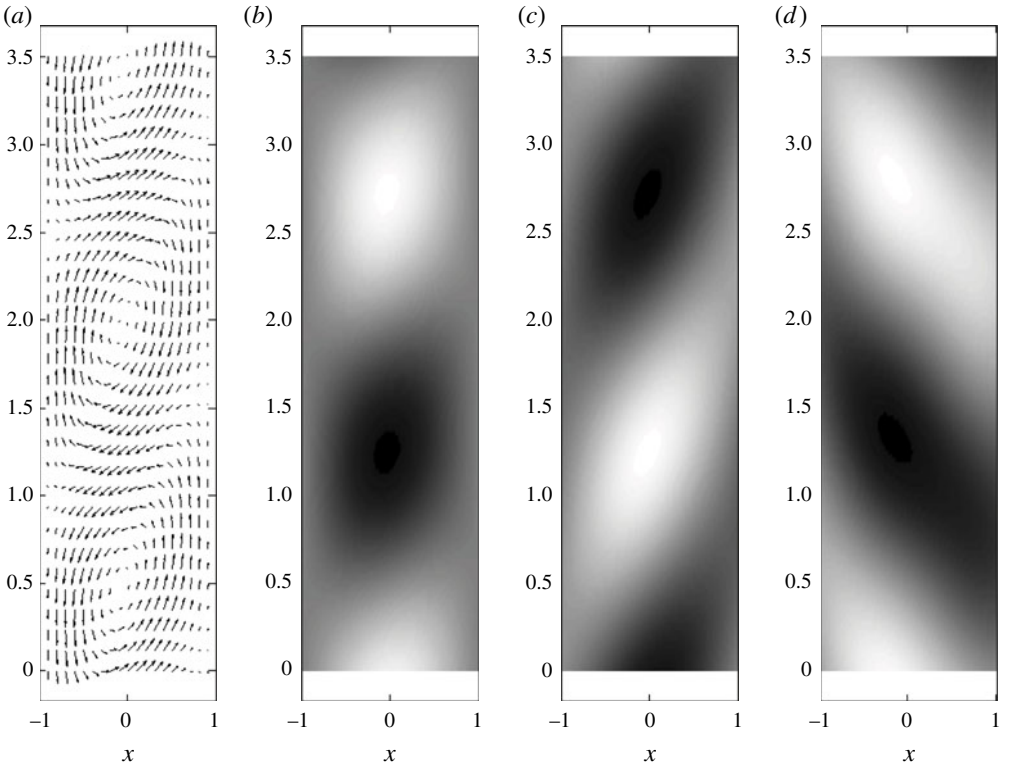

FIGURE 15. Same as figure 14 but for $\widetilde{Ra}_{mc} = 548.4$, $\widetilde{\alpha}_c = 2.135$, $\delta = 10°$.

8. Conclusions

In the current study the stability of a differentially heated layer of ferrofluid has been analysed and contrasted to that of a layer of paramagnetic fluid considered previously in Huang *et al.* (1997). The magnetic properties of a ferrofluid have been estimated using the experimental data and the modified mean field model that has been shown to be more accurate than the classical Langevin's law of magnetisation (Pshenichnikov 2007; Lebedev & Lysenko 2011). In contrast to the linear distribution of magnetic field that exists in a layer of a paramagnetic fluid, the magnetic field in a layer of a ferrofluid varies nonlinearly. The nonlinear distributions of unperturbed magnetic and magnetisation fields have been derived asymptotically and computed numerically for a range of fluid properties corresponding to realistic ferrofluids, including that used in previous experiments (Suslov *et al.* 2012). It has been shown that unlike in paramagnetic fluids such distributions in ferrofluids depend not only on the inclination of the applied magnetic field, but also on its magnitude.

The field nonlinearity found in ferrofluids is responsible for breaking the symmetry, which in turn results in several qualitative differences between instabilities detected in para- and ferromagnetic fluids. In particular, it is shown that in ferromagnetic fluids the instability arises preferentially near the hot wall bounding the layer. This is traced back to the curvature of the magnetic field lines inside a ferrofluid layer. The instability leading to the appearance of oblique and transverse rolls in a ferrofluid is found to be oscillatory, which is not the case in paramagnetic fluids.

Even though, similar to paramagnetic fluids, our linear stability analysis demonstrates that stationary longitudinal rolls are least stable, the possibility of the existence of propagating oblique and transverse rolls cannot be disregarded in experimental studies, especially those concerned with flows in finite geometries where the proximity of solid boundaries can suppress longitudinal rolls. The cited experimental observations indeed indicate that. Moreover, our preliminary results of weakly nonlinear analysis of perturbed thermomagnetic flows that will be reported elsewhere indicate that the bifurcation leading to the appearance of stationary longitudinal rolls is supercritical. However, this might not be the case for propagating oblique and transverse patterns where the degree of symmetry breaking is generally higher than for longitudinal rolls. Therefore it may be possible that the character of a bifurcation leading to non-stationary convection patterns could change to subcritical, at least in some parametric regions. In this case, in a realistic experiment, stationary longitudinal and finite-amplitude propagating oblique patterns can co-exist and interact. Even if it is confirmed that the bifurcation for travelling patterns remains supercritical so that non-stationary flow structures appear at necessarily larger governing parameters than the critical values for longitudinal rolls, they will still be experimentally observable in the form of time-dependent small-amplitude modulations of the main stationary structures once and thus cannot be disregarded.

Disturbance energy considerations have been used to determine that the physical cause of the detected instabilities is the variation of fluid magnetisation due to thermal disturbances. However, the related variation of a magnetic field is found to draw energy from the perturbed field, thus playing a stabilising role. It is also found that it is this magnetic field variation effect that determines the propagation direction of oblique and transverse instability patterns in a ferrofluid layer in inclined magnetic fields.

Acknowledgements

The authors would like to thank Professors G. F. Putin and A. A. Bozhko and Mr A. S. Sidorov of the Physics Department at Perm State National Research University, Russia for discussing the relevance of the presented computational results to the experimental studies currently conducted in their group.

REFERENCES

AGEIKIN, D. I. 1950 Determination of heat emission by means of thermomagnetic convection. *Proc. USSR Acad. Sci.* **74**, 229–232 (in Russian).

ALBRECHT, T., BÜHRER, C., FÄHNLE, M., MAIER, K., PLATZEK, D. & RESKE, J. 1997 First observation of ferromagnetism and ferromagnetic domains in a liquid metal. *Appl. Phys.* A **65**, 215–220.

ALTMEYER, S., HOFFMANN, CH., LESCHHORN, A. & LÜCKE, M. 2010 Influence of homogeneous magnetic fields on the flow of a ferrofluid in the Taylor–Couette system. *Phys. Rev.* E **82**, 016321.

BASHTOVOY, V. G., BERKOVSKY, B. M. & VISLOVICH, A. N. 1988 *Introduction to Thermomechanics of Magnetic Fluids*. Hemisphere.

BLUMS, E., CEBERS, A. O. & MAIOROV, M. M. 1997 *Magnetic Fluids*. Walter de Gruyter.

BOGATYREV, G. P. & GILEV, V. G. 1984 Concentration dependence of the viscosity of a magnetic liquid in an external field. *Magnetohydrodynamics* **20**, 249–252.

BOGATYREV, G. P. & SHAIDUROV, G. F. 1976 Convective stability of a horizontal layer of ferromagnetic fluid in a uniform magnetic field. *Magnetohydrodynamics* **3**, 137–146.

BOZHKO, A. A., PILUGINA, T. V., PUTIN, G. F., SHUPENIK, D. V. & SUHANOVSKY, A. N. 1998 On instability of thermogravitational flow in a ferrofluid vertical layer in the transversal magnetic field. In *Proceedings of the 8th International Conference on Magnetic Fluids, Plyos, Russia* (ed. Yu. Ya. Schelykalov), pp. 75–78. Ivanovo State Power University, Ivanovo, Russia.

BOZHKO, A. A. & PUTIN, G. F. 1991 Experimental investigation of thermo-magnetic convection in uniform external field. *Bull. Acad. Sci. USSR Phys. Series* **55**, 1149–1156.

BOZHKO, A. A. & PUTIN, G. F. 2003 Heat transfer and flow patterns in ferrofluid convection. *Magnetohydrodynamics* **39**, 147–169.

BOZHKO, A. A. & PUTIN, G. F. 2009 Thermomagnetic convection as a tool for heat and mass transfer control in nanosize materials under microgravity conditions. *Microgravity Sci. Technol.* **21**, 89–93.

BOZHKO, A. A., PUTIN, G. F., SIDOROV, A. S. & SUSLOV, S. A. 2013 Convection in a vertical layer of stratified magnetic fluid. *Magnetohydrodynamics* **49**, 143–152.

BOZHKO, A. A. & TYNJALA, T. 2005 Influence of gravitational sedimentation of magnetic particles on ferrofluid convection in experiments and numerical simulations. *J. Magn. Magn. Mater.* **289**, 281–285.

ELMORE, W. C. 1938 The magnetisation of ferromagnetic colloids. *Phys. Rev.* **54**, 1092–1095.

ENGLER, H., BORIN, D. & ODENBACH, S. 2009 Thermomagnetic convection influenced by the magnetoviscous effect. *J. Phys. Conf. Ser.* **149**, 012105.

FINLAYSON, B. A. 1970 Convective instability of ferromagnetic fluids. *J. Fluid Mech.* **40**, 753–767.

HART, J. E. 1971 Stability of the flow in a differentially heated inclined box. *J. Fluid Mech.* **47**, 547–576.

HATZIAVRAMIDIS, D. & KU, H.-C. 1985 An integral Chebyshev expansion method for boundary-value problems of O.D.E. type. *Comput. Maths Applics.* **11** (6), 581–586.

HENNENBERG, M., WESSOW, B., SLAVTCHEV, S., DESAIVE, TH. & SCHEILD, B. 2006 Steady flows of laterally heated ferrofluid layer: influence of inclined strong magnetic field and gravity level. *Phys. Fluids* **18**, 093602.

HUANG, J., EDWARDS, B. F. & GRAY, D. D 1997 Thermoconvective instability of paramagnetic fluids in a uniform magnetic field. *Phys. Fluids* **9**, 1819–1825.

IVANOV, A. O., KANTOROVICH, S. S., REZNIKOV, E. N., HOLM, C., PSHENICHNIKOV, A. F., LEBEDEV, A., CHREMOS, A. & CAMP, P. J. 2007 Magnetic properties of polydisperse ferrofluids: a critical comparison between experiment, theory, and computer simulation. *Phys. Rev.* E **75**, 061405.

KOJI, F., HIDEAKI, Y. & MASAHIRO, I. 2007 A mini heat transport device based on thermosensitive magnetic fluid. *Nanoscale Microscale Thermophys. Engng* **11**, 201–210.

KU, H.-C. & HATZIAVRAMIDIS, D. 1984 Chebyshev expansion methods for the solution of the extended Graetz problem. *J. Comput. Phys.* **56**, 495–512.

LANGE, A. 2004 Magnetic Soret effect: application of the ferrofluid dynamics theory. *Phys. Rev.* E **70**, 046308.

LEBEDEV, A. V. & LYSENKO, S. N. 2011 Magnetic fluids stabilized by polypropylene glycol. *J. Magn. Magn. Mater.* **323**, 1198–1202.

LIAN, W., XUAN, Y. & LI, Q. 2009 Design method of automatic energy transport devices based on the thermomagnetic effect of magnetic fluids. *Intl J. Heat Mass Transfer* **52**, 5451–5458.

MATLAB 2013 *Matlab R2013a*. The MathWorks, Inc., 3 Apple Drive, Natick, MA, USA.

MATSUKI, H. & MURAKAMI, K. 1987 Performance of an automatic cooling device using a temperature-sensitive magnetic fluid. *J. Magn. Magn. Mater.* **6**, 363–365.

MUKHOPADHYAY, A., GANGULY, R., SEN, S. & PURI, I. K. 2005 A scaling analysis to characterize thermomagnetic convection. *Intl J. Heat Mass Transfer* **48**, 3485–3492.

ODENBACH, S. 1995 Microgravity experiments on thermomagnetic convection in magnetic fluids. *J. Magn. Magn. Mater.* **149**, 155–157.

ODENBACH, S. 2002*a* *Ferrofluids: Magnetically Controllable Fluids and Their Applications*. Springer.

ODENBACH, S. 2002*b* *Magnetoviscous Effects in Ferrofluids*. Springer.

ODENBACH, S. 2004 Recent progress in magnetic fluid research. *J. Phys.: Condens. Matter* **16**, R1135–R1150.

ODENBACH, S. 2009 *Colloidal Magnetic Fluids: Basics, Development and Applications of Ferrofluids*, Lecture Notes in Physics. Springer.

ODENBACH, S. & MÜLLER, H. W. 2005 On the microscopic interpretation of the coupling of the symmetric velocity gradient to the magnetization relaxation. *J. Magn. Magn. Mater.* **289**, 242–245.

ODENBACH, S. & RAJ, K. 2000 The influence of large particles and agglomerates on the magnetoviscous effect in ferrofluids. *Magnetohydrodynamics* **36** (4), 312–319.

POP, L. M. & ODENBACH, S. 2006 Investigation of microscopic reason for the magnetoviscous effect in ferrofluid studied by small angle neutron scattering. *J. Phys.: Condens. Matter* **18**, S2785–S2802.

PSHENICHNIKOV, A. F. 2007 A mutual-inductance bridge for analysis of magnetic fluids. *Instrum. Exp. Tech.* **50**, 509–514.

ROSENSWEIG, R. E. 1979 Fluid dynamics and science of magnetic fluids. *Adv. Electron. Electron Phys.* **48**, 103–199.

ROSENSWEIG, R. E. 1985 *Ferrohydrodynamics*. Cambridge University Press.

RYSKIN, A. & PLEINER, H. 2004 Influence of a magnetic field on the Soret-effect-dominated thermal convection in ferrofluids. *Phys. Rev.* E **69**, 046301.

RYSKIN, A. & PLEINER, H. 2007 Magnetic-field-driven instability in stratified ferrofluids. *Phys. Rev.* E **75**, 056303.

SCHWAB, L., HILDEBRANDT, U. & STIERSTADT, K. 1983 Magnetic Bénard convection. *J. Magn. Magn. Mater.* **39**, 113–114.

SUSLOV, S. A. 2008 Thermo-magnetic convection in a vertical layer of ferromagnetic fluid. *Phys. Fluids* **20** (8), 084101.

SUSLOV, S. A., BOZHKO, A. A. & PUTIN, G. F. 2008 Thermo-magneto-convective instabilities in a vertical layer of ferro-magnetic fluid. In *Proceedings of the XXXVI International Summer School–Conference 'Advanced Problems in Mechanics', Repino, Russia* (ed. D. A. Indeitsev & A. M. Krivtsov), pp. 644–651. Institute of Problems of Mechanics of the Russian Academy of Sciences, St. Petersburg, Russia.

SUSLOV, S. A., BOZHKO, A. A., PUTIN, G. F. & SIDOROV, A. S. 2010 Interaction of gravitational and magnetic mechanisms of convection in a vertical layer of a magnetic fluid. *Phys. Proc.* **9**, 167–170.

SUSLOV, S. A., BOZHKO, A. A., SIDOROV, A. S. & PUTIN, G. F. 2012 Thermomagnetic convective flows in a vertical layer of ferrocolloid: perturbation energy analysis and experimental study. *Phys. Rev.* E **86**, 016301.

SUSLOV, S. A. & PAOLUCCI, S. 1995*a* Stability of mixed-convection flow in a tall vertical channel under non-Boussinesq conditions. *J. Fluid Mech.* **302**, 91–115.

SUSLOV, S. A. & PAOLUCCI, S. 1995*b* Stability of natural convection flow in a tall vertical enclosure under non-Boussinesq conditions. *Intl J. Heat Mass Transfer* **38**, 2143–2157.

TAGG, R. & WEIDMAN, P. D. 2007 Linear stability of radially-heated circular Couette flow with simulated radial gravity. *Z. Angew. Math. Phys.* **58**, 431–456.

TANGTHIENG, C., FINLAYSON, B. A., MAULBETSCH, J. & CADER, T. 1999 Heat transfer enhancement in ferrofluids subjected to steady magnetic fields. *J. Magn. Magn. Mater.* **201**, 252–255.

TSEBERS, A. O. 1982 Thermodynamic stability of magnetofluids. *Magnetohydrodynamics* **18**, 137–142.

VÖLKER, T. & ODENBACH, S. 2003 The influence of a uniform magnetic field on the Soret coefficient of magnetic nanoparticles. *Phys. Fluids* **15**, 2198–2207.

WEISS, P. 1907 L'hypothèse du champ moléculaire et la propriété ferromagnétique. *J. Phys. Theor. Appl.* **6**, 661–690.

ZABLOTSKY, D., MEZULIS, A. & BLUMS, E. 2009 Surface cooling based on thermomagnetic convection: numerical simulation and experiment. *Intl J. Heat Mass Transfer* **52**, 5302–5308.

ZEBIB, A. 1996 Thermal convection in a magnetic fluid. *J. Fluid Mech.* **321**, 121–136.